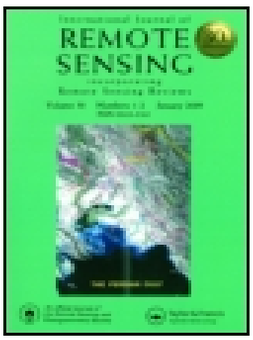

International Journal of Remote Sensing

ISSN: 0143-1161 (Print) 1366-5901 (Online) Journal homepage: http://www.tandfonline.com/loi/tres20

Estimation of sea state from Sentinel-1 Synthetic aperture radar imagery for maritime situation awareness

Andrey Pleskachevsky, Sven Jacobsen, Björn Tings & Egbert Schwarz

To cite this article: Andrey Pleskachevsky, Sven Jacobsen, Björn Tings & Egbert Schwarz (2019): Estimation of sea state from Sentinel-1 Synthetic aperture radar imagery for maritime situation awareness, International Journal of Remote Sensing, DOI: 10.1080/01431161.2018.1558377

To link to this article: https://doi.org/10.1080/01431161.2018.1558377

Published online: 17 Jan 2019.

INTERNATIONAL JOURNAL OF REMOTE SENSING
https://doi.org/10.1080/01431161.2018.1558377

Taylor & Francis
Taylor & Francis Group

Estimation of sea state from Sentinel-1 Synthetic aperture radar imagery for maritime situation awareness

Andrey Pleskachevsky, Sven Jacobsen, Björn Tings and Egbert Schwarz

Remote Sensing Technology Institute, Maritime Safety and Security Lab, German Aerospace Center (DLR), Bremen, Germany

ABSTRACT

A new empirical algorithm CWAVE_S1-IW for estimation of significant wave height H_s including swell and wind sea from C-band satellite-borne Synthetic Aperture Radar (SAR) data has been developed for Sentinel-1 (S1) Interferometric Wide Swatrh Mode (IW) imagery. The algorithm was implemented into the Sea Sate Processor (SSP) for fully automatic processing for near real time (NRT) services and allow the estimation of wave fields of thousands of kilometres in the flight direction and 250 km swath from S1 IW scenes consisting of a sequence of individual images.

The priority of CWAVE_S1-IW development was an automatic, fast and robust raster processing independent of wave patterns, applicable even when only clutter is visible in the SAR images. The algorithm is based on the spectral analysis of subscenes in wavenumber space. The empirical function allows direct H_s estimation from image spectra without first converting them into wave spectra and uses integrated image spectra parameters as well as estimated local wind information. A texture analysis based on Grey Level Co-occurrence Matrices (GLCM) is also applied. In this way, also the parameters of short waves can be estimated, which are not visible in S1 IW images and are only represented by clutter.

The algorithm was tuned worldwide using *in-situ* collocated measurements of 92 buoys with more than 2500 acquisitions. The validated SSP allows automatic processing of worldwide S1 IW images in VV or HH polarization, including Atlantic storms, cyclones, and huge storms in the Gulf of Alaska with a root-mean-square (RMSE) error of 80 cm for H_s. For the closed seas like the North Sea, Baltic Seas and Black Sea the accuracy is higher with an RMSE = 55 cm. The algorithm is integrated into a demonstration service, used for further validation at the DLR ground station in Neustrelitz. The NRT processing has been tested by supporting a research ship cruise in the Antarctic Sea.

ARTICLE HISTORY
Received 16 March 2018
Accepted 23 November 2018

1. Introduction

This paper introduces a new algorithm and processor for meteo-marine parameter estimation from Sentinel-1 (S1) imagery. The Interferometric Wide Swath Mode (IW) covers area-strips of thousands of kilometres of earth and ocean surface with 10 m pixel resolution in sequences of multiple individual IW images with an approximate size of 200 km × 250 km. The worldwide

CONTACT Andrey Pleskachevsky Andrey.Pleskachevsky@dlr.de

acquisitions with high revisit frequency are free for common use and allow unprecedented opportunities for the observation of ocean processes and natural features. However, the nature of S1 C-Band imagery for moving targets under relatively coarse resolution imposes a limit for imaging of ocean waves: only long wave structures with wavelengths longer than ca. 120 m can be clearly seen in the IW images; shorter waves or waves with amplitude above ca. 5 m under strong winds are imaged as clutter. To return the correct wave height for the whole range of sea state conditions, the traditional method of considering image spectra was extended by the implementation of image features analysis using a Grey Level Co-occurrence Matrix (GLCM).

The paper addresses in the first place the SAR oceanography community and users of remote sensing information such as meteorological offices. Figure 1 shows the possibilities

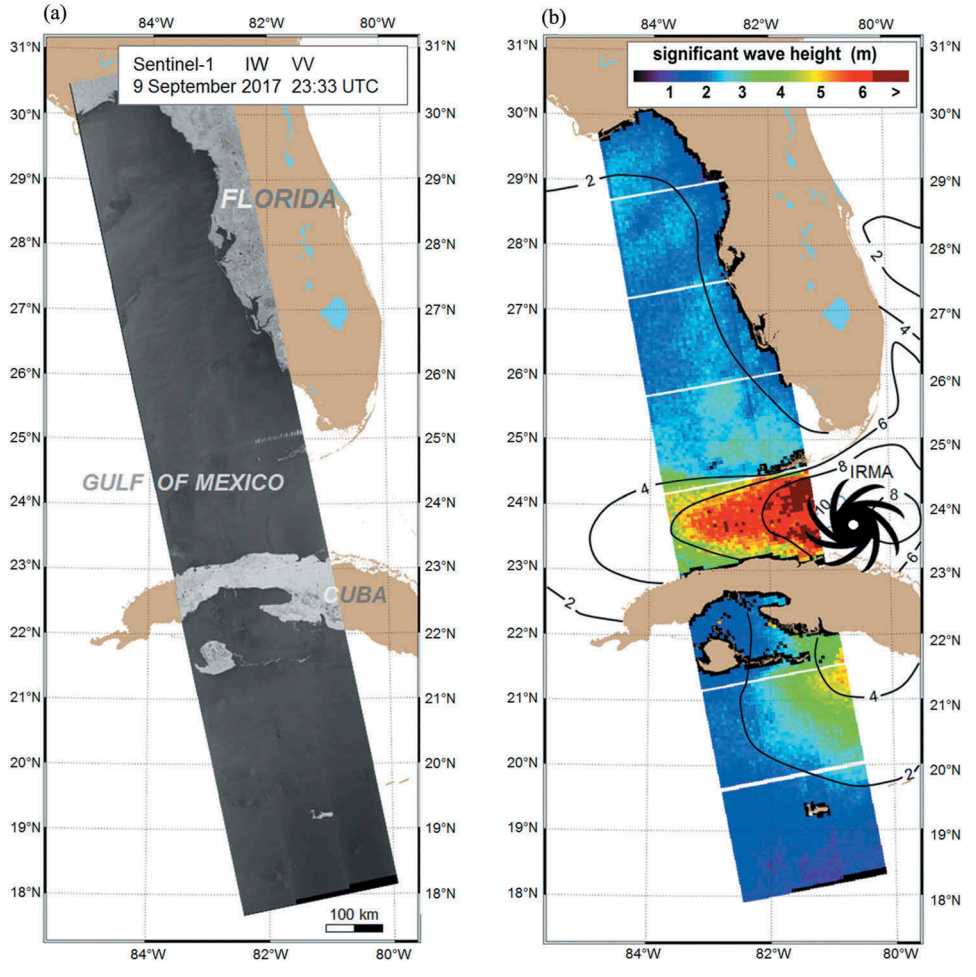

Figure 1. Example of significant wave height H_s processed with 6 km posting using the Sea State Processor with empirical CWAVE_S1-IW algorithm developed in this study. (a) Sentinel-1 IW scene consists of eight individual images and acquired over Cuba and Florida on 9 September 2017 at 23:33 UTC while hurricane 'Irma' was moving towards the Gulf of Mexico. (b) H_s is estimated, the isolines present the WWIII model results for H_s (NOAA).

of the developed tool by an S1 IW scene acquired while hurricane 'Irma' was moving towards the Gulf of Mexico. Based on these results, ESA reported on the new possibilities for tracking storms and hurricanes that open with the development of algorithms in such unusual cases: 'Importantly, this information about the state of the sea can help to assess how destructive a hurricane is and predict its path – and, therefore, where and when it is likely to make landfall. The same information can also be used to warn ships and to issue warnings of coastal flooding. This new technique was used for the first time when hurricane Irma struck Cuba and the Florida Keys in early September. Here, waves up to 10 m high were measured…. This is especially important because *in-situ* measurements of wind and sea state cannot be gained from buoys or dropped probes in such extreme weather or over such a wide area.' (ESA 2017).

The algorithm developed in this study was also integrated into a processor as part of a near-real-time (NRT) demonstrator service for support of Maritime Situation Awareness (MSA) at the DLR Ground Station Neustrelitz. This scientific service involves the daily provision of surface wind and sea state parameters estimated fully automatically from S1 IW images for the North and Baltic Seas.

1.1. *Synthetic aperture radar for sea state estimation*

Spaceborne Synthetic Aperture Radar (SAR) is an active microwave remote sensing instrument providing two-dimensional (2D) information of the normalised radar cross section σ_o (NRCS), which represents the ability of a surface to reflect the radar signal. The backscatter is governed by the surface roughness on the scale of the radar wavelength (5.6 cm for S1 C-band radar). In the case of long surface waves and low wind conditions, the radar return echo is dominated by so-called Bragg scattering of short ripple capillary waves with a dimension of order centimetres, which are produced by wind striking the sea surface. Under strong wind conditions a series of additional backscattering take place, e.g. the individual wind waves are steep enough to produce direct reflections and also break.

Due to independence from sunlight and cloudiness, global coverage and high resolution, remote sensing SAR data is an indispensable source of 2D information on the ocean surface for the open sea and coastal applications (e.g. Lehner, et al. 2013). The rapid development of satellite techniques, SAR sensors, SAR processors, algorithms and ground infrastructures made possible a series of oceanographic applications in NRT in recent years (Schwarz, et al. 2015). Several minutes after the acquisition, the derived products can be transferred to weather services for validation of their forecasting models (Pleskachevsky, Rosenthal, and Lehner, 2016). The different products such as significant wave height H_s, surface wind speed U_{10}, ice coverage, oil spills, etc., can be processed in parallel for the same image data and combined for supporting MSA.

1.2. *Maritime situational awareness MSA and sentinel SAR*

Generally, under MSA one understands a system for the fusion of various data in order to improve the safety of navigation. This includes information on:

— the maritime environment; local sea state, coastal lines and sandbars, ice coverage, etc., based on remote sensing, *in-situ* measurements and forecast modelling. Information on pollution (e.g., oil slicks) is also a part of this topic,

— ship traffic information (ship location, speed, ship's Automatic Identification System (AIS) messages).

MSA services have been developed worldwide with remote sensing data based on SAR techniques as one of the most important parts (Lehner, et al. 2014).

The majority of the global transportation of goods takes place over the oceans, justifying the need for safe and secure navigation. Maritime surveillance is nowadays of global importance. SAR satellite systems are one of the key elements because of the possibility to derive marine information from the large areas covered by wide swath imaging modes independent of sun illumination and cloudiness. The increased number of space systems available for remote sensing applications enables ocean monitoring tasks in higher spatial and temporal resolution. Furthermore, the European Earth Observation Programme 'Copernicus' provides free and open data access and this stimulates the development of new applications in the maritime domain.

The combination of different pieces of information such as ship positions, local sea state, wind fields, coastline and ice coverage in a single MSA platform represents a powerful tool to monitor both environmental and safety or security concerns in the maritime domain. For example, S1 IW imagery allows two acquisitions per day (ascending and descending orbits) of certain regions, e.g. the North Sea or the Black Sea. Hence, storm development and propagation can be tracked and evaluated directly onboard a ship by comparing the forecast results (e.g. from WWIII wave model from NOAA) with NRT wave height products estimated from S1 IW imagery and with online *in-situ* buoy measurements (if available). Correspondingly, the course of ships can be corrected using the projected motion of the storm peak. A concrete case will be discussed in Section 4.2 with an example storm that occurred in the Black Sea in 2017 using tools developed in this study.

Another application of a reliable MSA is gaining importance with increasing offshore construction and maintenance activities. Offshore construction, e.g. in the Offshore Wind business or pipeline construction is often limited by sea state conditions, either by feasibility of the operation itself or insurance safety margins. Scheduled activities regularly have to be postponed by days due to unfavourable weather conditions. However, the decision whether to discard planned operations for the day and stay in the harbour is based on weather forecasts. As forecast values for wind or sea state are not 100% precise, a safety margin is applied to avoid futile navigation to the construction site or to safely stay within insurance margins. Here NRT MSA data represents a tool to check the accuracy of the daily weather forecast in terms of meteorological parameters or to verify the position of fronts with respect to the forecast data. Due to prior and more accurate knowledge of the conditions at the construction site and a more reliable evaluation of the forecast quality on a daily basis, this procedure will eventually save costs as fewer operations will have to be cancelled after the trip to the construction site, and some operations can be carried out despite an unfavourable, but inaccurate, forecast.

1.3. *Sea state estimation from SAR imagery*

Ocean surface measurements have a long history and been carried out using SAR data since the first spaceborne SAR missions. They include such well-known missions as L-band SAR SEASAT launched in 1978, C-Band European Radar Satellites ERS-1 and ERS-2 launched in 1991 and 1995, ENVISAT (Environmental Satellite) with C-Band Advanced Synthetic Aperture Radar (ASAR) in 2002 and others. Different inversion schemes, e.g. Hasselmann, and Hasselmann, (1991), Krogstad, (1992), Engen, and Johnson, (1995), Hasselmann, et al. (1996), Mastenbroek, and de Valk (2000), Chapron, Johnsen, and Garello, (2001), Schulz-Stellenfleth, Lehner, and Hoja, (2005), Collard, Ardhuin, and Chapron, (2009) were developed in order to estimate wave spectra and sea state parameters from SAR data.

The estimation of the sea state parameters from the SAR images traditionally uses the Fast Fourier Transformation (FFT) of a subscene. Further, the image spectrum is employed, which can be done in two different ways:

(1) Developing transfer functions for the reconstruction of wave spectra (Alpers, and Rufenach, 1979) followed by integration and estimation of the integrated parameters.
(2) Direct estimation of the sea state parameters by empirical model functions (EMFs) from image spectra without transformation (Lehner, Pleskachevsky, and Bruck, 2012, Bruck, and Lehner, 2015, Pleskachevsky, Rosenthal, and Lehner, 2016).

The first approach is more suitable for the estimation of swell-spectra and can be of interest to the spectral wave modelling. It can be successfully applied in the case where long waves are recorded in the open ocean. Understanding the mechanism of SAR-imaging of the ocean surface waves plays a key role here. Nevertheless, the method needs a homogenous sea state field imaged without artefacts and thereby works with scenes that pass the homogeneity check by comparison of the variance with the mean. The second limitation concerns the length of the acquired sea state. The ocean waves propagating in the azimuth direction must be longer than the so-called *cutoff* (Alpers et al., 1986, Holt, 2004) of about 120 m for S1 IW: shorter waves are not visible in the resulting SAR-images and consequently cannot be transferred into wave spectra. For example, even in the case of ENVISAT ASAR Wave Mode (covering ca. 10 km ×5 km with 30 m × 30 m resolution along the orbit every 100 km) acquired over open ocean with well pronounced long waves, about 20% of images failed to pass the homogeneity test and cannot be used (Schulz-Stellenfleth, König, and Lehner, 2007, Li, Lehner, and Bruns, 2011). Additionally, as a series of artefacts (ships, offshore constructions, currents and wind fronts, shallow bathymetry influences) are often present in SAR images. For example, in the North Sea, only about 20–25% of the S1 IW images contain subscenes that can be used for spectral transformations (results from this study). All of these limitations fall away by applying the second method, but they need special treatment. Furthermore, the empirical functions require less computation time in comparison to mathematical iterations of the first approach. Such iterations can take hours and can hardly be used for NRT purposes where thousands of subscenes must be processed within a few minutes. The empirical functions are also more suitable for short wind-sea waves and noisy images. Although in some cases with well pronounced swell waves the accuracy may be lower than using transfer functions, in

other cases, where the mathematical methods do not work, it is the only a way to get quick, reliable results. The fast and robust estimation of parameters using this approach allows automatic and trustworthy processing in the raster of all acquired images by fulfilling NRT requirements, while only about ca. 0.5% of the data (subscenes) must be discarded. The discarded data present extreme processing conditions where the complete subscene is contaminated with disturbing radar echo signals caused, e.g. by rain cells, wind farms with numerous of turbines, groups of ships, and massive wave breaking in shallows (e.g. over reefs and sandbars). (Pleskachevsky, Rosenthal, and Lehner, 2016, Rikka, et al. 2018a, 2018b. and also this study).

Since launching satellites S1A in 2014 and S1B in 2016 a series of investigations for S1 SAR imagery have been carried out worldwide for different S1 modes. For example, an iterative nonlinear algorithm to estimate phase-resolved deterministic maps of wave-induced orbital velocities, from which elevation spectra were derived over ice-covered regions for wave mode images, was demonstrated by Ardhuin, et al. (2016). The S1 Wave Mode (WV) acquires data in 20 km × 20 km vignettes, at 5 m × 5 m spatial resolution, every 100 km along the orbit. Sun, et al. (2018) presents a data assimilation for a spectral wave model using the S1 WV. Also, Stopa and Moushe 2017 published empirical algorithms developed for S1 WV. A semi-empirical algorithm for H_s and mean wave period retrieval from VV S1 Stripmap (SM, swath width of 80 km, 5 m × 5 m spatial resolution) was also reported by Shao, et al. (2016). However, all these methods are concentrated on WV and SM modes, where due to the higher resolution, the sea state details are sufficiently imaged at the cost of smaller coverage. The sequence of IW mode images with 250 km swath can cover an ocean surface strip about 2000 km and offers more opportunities for global MSA and have been considered in this study.

1.4. *Objective*

The objective of this study was developing the algorithm for total significant wave height (including swell and wind sea) H_s estimation from S1 IW imagery appropriate for NRT and a practical tool for robust automatic processing of data operationally. The requirement for function development was the operating capability for all kinds of sea state (short wind sea, swell, very high waves with long overhanging crests, their combination) with the desired accuracy defined by a root-mean-square error (RMSE) of fewer than 1 m for H_s. These conditions are determined by the accuracy shown by algorithms based on SAR data which have reached an RMSE in the interval ca. 0.5–1.2 m by comparison with *in-situ* measurements. For example in Stopa, and Mouche, (2017) RMSE = 0.60 m, in Shao, et al. (2016) RMSE = 0.69 m, and in Li, Lehner, and Bruns, (2011) RMSE = 0.70 m are reported. Since the aim of the investigation was not only theoretical, but ultimately practical, a compatibility with the architecture of the sea state processor SSP already developed for TerraSAR-X (TS-X) imagery and working in NRT at the ground station in Neustrelitz (Pleskachevsky, Rosenthal, and Lehner, 2016) had a high priority.

The development of an EMF and a working tool included three tasks:

(1) Designing the CWAVE_S1-IW EMF based on direct estimation of integrated sea state parameters from SAR image spectra without transformation into wave spectra.

(2) Integrating the CWAVE_S1-IW into the SSP installed in the NRT chain at the satellite ground station "Neustrelitz" and already adopted for TS-X SM sea state processing. Extended in the framework of this study, SSP is currently working not only with TS-X SM but also with S1 IW and includes procedures for reading, calibrating, landmasking, filtering of artefacts, XWAVE_C (for TS-X SM)/ CWAVE_S1-IW, wind estimation, quality control of results, and common and special-points outputs. The SSP also includes a user interface for parameter input and control and sequentially performs stable raster analysis of multiple images using the newest NRT acquisitions as well as images from the archive (Pleskachevsky, Rosenthal, and Lehner, 2016).
(3) Collecting and processing the data for different regions and weather condition as well as investigation of interesting individual and extraordinary cases, e.g. while hurricane "Irma" was moving towards the Gulf of Mexico and the Florida coast; analysis of results, verification and validation of the algorithm. A special item was SSP testing for real needs by supporting scientific vessel cruises in NRT.

2. Data and methodology

In this section, the data used are described. Surface wave imaging in S1 IW imagery, technical improvements of the SSP and EMF to estimate sea state parameters are discussed.

2.1. *Sentinel-1 IW images for sea state estimation*

Copernicus C-band satellites Sentinel-1A and Sentinel-1B were launched in 2014 and 2016 respectively and operate at an altitude of 704 km with a ground speed of 6.8 km s^{-1}. The IW mode combines a large swath width with a moderate geometric resolution. The individual IW (GRDH: level-1 Ground Range Detected High-resolution products) images cover approximately 200 km in the azimuth and 250 km in range directions. The original products are available in single (HH or VV) or dual polarisation (HH+HV or VV+VH). For the sea state estimation, the VV or HH polarization image data were used. The NRCS σ_o is first calculated from the pixel's digital number $I(x,y)$:

$$\sigma_o(x,y) = \frac{I(x,y)^2}{k_s^2} \tag{1}$$

where k_s is the calibration factor given for the pixel (specified by the manufacturer ESA), y and x are image coordinates in azimuth (flight) and range, respectively. The SAR image analysis is based on Fast Fourier Transformation (FFT) of subscenes which provides image spectra in wavenumber space. The value of each pixel $\sigma_o(x,y)$ of the subscene is normalized, resulting in a value $\sigma_c(x,y)$ used henceforward for sea state estimations:

$$\sigma_c(x,y) = \frac{\sigma_o(x,y) - \sigma_o}{\sigma_o} \tag{2}$$

where σ_o is the mean value of the NRCS for the subscene. The idea behind this is to define a common procedure in order to separate the local NRCS modulation due to sea

state from the mean NRCS value due to the local wind speed in a SAR subscene (e.g. Schulz-Stellenfleth, König, and Lehner, 2007). However, in comparison to ocean waves which present a symmetric oscillation of the surface at crest and trough (true for swell waves approximated using linear wave theory), the SAR imaged wave patterns with max and min NRCS values do not represent the real wave shape even in the simple case of long swell. The maximal image brightness does not correspond to the highest point of the local surface elevation, but to its optimal reflection depending on a series of factors like the incidence angle and wave propagation direction. Similarly, the reduction of the radar signal reflection in the shadowed part of the wave does not represent a *sine* function-like surface oscillation by real waves such that no symmetry in the signal intensity occurs (e.g. Holt, 2004). Under real conditions, the SAR image is influenced also by short wind waves developed under local winds. These are not resolved and therefore not directly visible in the SAR IW images, but amplify the radar echo signal, produce an additional noise, and influence the energy in the image spectra. From this, one can see, an offset connected to the local wind speed is required for H_s estimation based on σ_o (for details on the EMF, see section 2.7).

Ocean surface gravity waves are moving targets. Hence, the mechanisms producing their SAR backscatter consist of the linear transformation of tilt and hydrodynamic modulation, as well as non-linear distortions described in the literature (e.g. Alpers, and Rufenach, 1979, Hasselmann, et al. 1985). This leads to, among other effects, image smearing and a loss of information beyond the so-called azimuth *cutoff* wavelength. This effect is associated with the so-called *velocity bunching* meaning shifted imaging of moving wave-facets by the Doppler effect. In a resulting SAR image, a moving target is displayed shifted from its real position in the SAR flight direction y proportional to its velocity u_r towards the sensor. For example, in the case of S1 with a platform velocity of V_{SAR} = 6.8 km s^{-1}, a target moving with radial speed u_r = 1 m s^{-1} will be displaced by $D_y = (u_r/V_{SAR})\times R_o$ (Lyzenga, Shuchman, and Lyden, 1985), $D_y \approx$ 135 m for a radar signal incidence angle $\theta = 40°$ and corresponding slant range R_o of ca. 9.2 $\times 10^5$ m (this value is about a factor of two larger than for TS-X due to the higher orbit). In case D_y is larger than one wavelength, the imaging regime is called strongly nonlinear: azimuth travelling waves are no longer visible. The minimal visible wavelength for azimuth travelling waves observed for S1 IW images is about 120–150 m. This corresponds roughly to a *cutoff* estimation using a simple empirical formula given in (Holt, 2004):

$$L_{min} = C_0 \frac{R_o}{V_{SAR}} H_s^{0.5} \tag{3}$$

where L_{min} is the minimum detectable azimuth *cutoff* wavelength, C_0 is a constant of order 1 with unit $m^{0.5} \times s^{-1}$ For swell waves with a H_s of 1 m and for R_o corresponding to $\theta = 40°$ the *cutoff* wavelength $L_{min} \approx$ 135 m according to Equation.3.

Generally, according to this study, three typical sea state conditions (three sea state classes) can be distinguished in S1 IW imagery requiring separate consideration:

(1) Low and short sea state with H_s under ca. 1.5 m and peak wavelength L_p under ca. 100 m. This sea state is imaged typically as noise, no wave-like pattern can be seen in S1 IW. The image spectra are noisy without prominent peaks.

(2) Long waves with L_p longer than ca. 120 m (low and moderate wind). Independent of the nonlinearity of SAR imaging, the wave structures are visible in S1 IW. The image spectra depict energy connected to swell waves and consist of prominent peaks.
(3) Storm condition with strong winds >15 m s^{-1} (Beaufort scale 7 and more). In the ocean, this corresponds mostly to waves higher than ca. 5 m H_s with two systems: swell waves in the background and local steep wind waves superimposed on them. Under such conditions, as can be seen from this study, the steep local wind sea waves break and their imaging hinders the imaging of swell waves in the background. In the resulting S1 IW image, the wave-l patterns are hardly visible.

Today, with the operation of high-resolution SARs (e.g. TS-X, COSMO-Skymed), comparison with the coarser resolution S1 sensor helps answer a series of questions about SAR wave imaging. Figure 2 shows example images of the sea state for calm, moderate and strong conditions for S1 IW C-band and TS-X StripMap X-band. These typical subscenes with a coverage of 2.5 km × 2.5 km in the flight direction come from scenes acquired in the North Atlantic and the North Sea in VV polarization.

As seen in Figure 2, only under moderate conditions the wave patterns (swell) are visible in S1 IW, while in TS-X SM waves are visible in one or another way for all

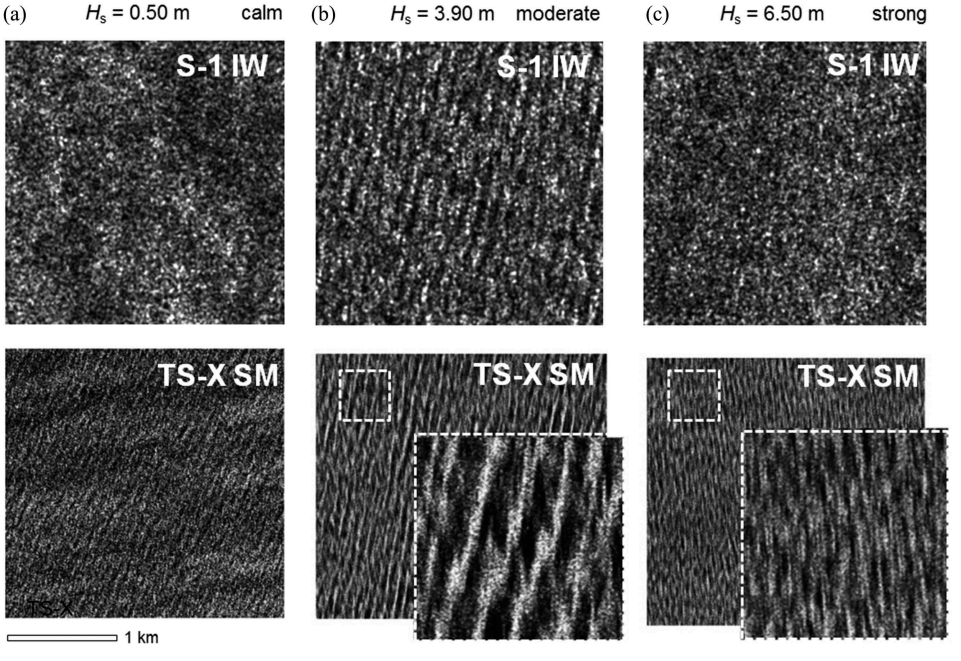

Figure 2. Examples for imaging of sea state for calm (a), moderate (b) and strong conditions (b) for Sentinel-1 IW C-band (first row) and TerraSAR-X StripMap (SM) X-band images (second row). The subscenes 2.5 km × 2.5 km in flight direction VV polarization are shown. Only for the moderate condition (middle), the wave pattern is clearly visible for S1 IW, while in TS-X StripMap these are visible under all conditions. Nonlinear effects like smoothing streaks on TS-X images help to classify conditions like a wave breaking. For S1 IW this option is not available, which justifies the need to include the additional information.

presented conditions (L_p > ca. 60 m). For S1 IW, for both calm and strong cases, the waves 'invisibility' occurs on account of the stronger non-linear effects (velocity bunching) due to the higher satellite altitude (in comparison to TS-X) and the coarser resolution. In the first case, the small and short wind waves cannot be resolved in their original form (see *cutoff* above). In the second case, under strong local winds, the wind sea-waves cover the swell-waves and their smeared imaging obscures the swell structures. Moreover, an additional radar echo is produced by strong wave breaking with additional image noise obscuring the swell signatures. Note, for TS-X altitude and SM resolution of 1.2 m pixel size these structures are presented by streaks which allow the detection of swell structures below them. This smoothing-streak effect in TS-X SM images helps to classify wave breaking. Due to differences between X-band and C-band, but more due to coarse resolution and altitude, this option is not available for S1 IW. As became clear in this study, additional information independent of the classical FFT analysis was needed to recognise the waves for calm and strong conditions producing similar spectra.

2.2. *Area of the investigation, measurement data and collocations*

The background of this study is the development of a processor capable of working worldwide in NRT. However, the accuracy of a general worldwide data comparison does not represent the accuracy of conditions at different real locations. Various kinds of sea state dominate in different regions, show diverse SAR imaging and cannot be estimated with the same accuracy.

Initially, the North Sea and eastern Baltic Sea with roughly 30 buoys collocated with about 600 acquisitions in 2014–2015 were used for the tuning of the algorithm. The dataset contained all S1 IW images acquired in the area (Copernicus Open Access Hub, DataHub). The mean H_s amounted to ca. 0.90 m and individual values rarely exceeded 4 m. In order to cover the domain of H_s > 4 m, storm conditions were additionally found and added to the dataset for 2015. Later, all acquisitions in the North Atlantic collocated with measurements (mostly from oil platforms) were also processed and included into the tuning dataset. Next, the west and east coasts of USA and Canada were included, collocated with about 40 NDBC NOAA buoys. Finally, acquisitions over the Aleutian Islands and Hawaii were added. Table 1 shows the locations and acquisitions used for tuning and validation of the algorithm (the validation process is ongoing as the number of images increases weekly. Therefore, the numbers in the table are rounded and represent the minimal number of considered images at the time of paper submission). Figure 3 presents an overview of typical collocations with individual S1 IW images used for algorithm tuning in the North Sea, Eastern Baltic and North Atlantic.

The measurement data were collected using a series of data sources:

- National Data Buoy Center (NOAA),
- European Marine Observation and Data Network (EMODnet),
- North West Shelf Data Portal (NWSPORTAL),
- Marine Environmental Monitoring Network in the North Sea and Baltic Sea (MARnet),
- COSYNA data web portal (CODM),

Table 1. Number of Sentinel-1 IW images used for collocation with sea state measurements worldwide.

Area	buoys in region	tuning images processed	validation images processed
North Sea (south)	27	463	570
North Sea (north)	9	385	400
Baltic Sea (west)	5	24	50
Baltic Sea (east, inc. Gulf of Finland)	4	28	30
North Atlantic (inc. Bay of Biscay)	26	493	250
USA/Canada west coast	25	378	20
USA/Canada east coast	37	365	20
Aleutian Islands	2	54	10
Hawaii	4	49	5
Total	139	2239	1355

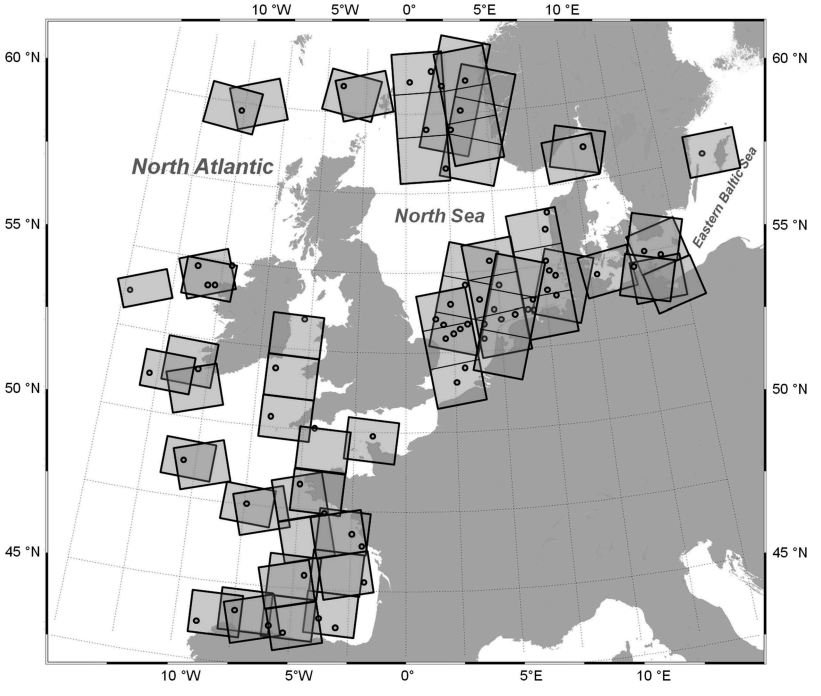

Figure 3. Example of collocations of individual S1 IW images with measurement stations (circles) in the North Sea, Eastern Baltic and North Atlantic used for algorithm tuning and validation.

- national weather service of Germany (BSH),
- national weather service Sweden (SMHI) and Estonia (MSI).

The spatial collocation was done by evaluating the distance between the centre-coordinates of all subscenes in an image and the coordinate of the respective measurement equipment. An active subscene with the minimum distance to the equipment coordinate was selected as collocated. The collocation distance applied was less than

5 km for the North Sea (subscene size 2.5 km) due to local variability in coastal regions and less than 20 km for the open Atlantic where the local variability is lower. For the temporal collocation, an interpolation in time was necessary, especially for storm conditions where the H_s rapidly changes at the measurement location in the magnitude of meters during a few tens of minutes. A typical situation observed at Oil Platforms in the North part of the North Sea, e.g. North-Cormorant (oilfield located 160 km north-east of Lerwick, Shetland Island), is that H_s decreases from 8 m up to 4 m during the only 1 h after the storm peak has passed and propagates along the North Sea mostly towards German Bight.

2.3. *Sea state processor for sentinel-1 IW*

In general, a model function estimates a parameter under certain conditions and limitations. Beyond the scope of the function domain, the data cannot be interpreted correctly. Therefore, a check of the data is usually applied, e.g. homogeneity test (e.g. Li, Lehner, and Bruns, 2011), to select the data satisfying the function domain. In order to increase the amount of appropriate data, a series of operations must be additionally applied before the model function can be invoked and the results can be considered trustworthy. For raster sea state estimation using the empirical XWAVE (X-band) or CWAVE (C-band) functions a comprehensive infrastructure is needed, including data preparation, artefacts filtering, a combination of estimated sea surface wind, GLCM as well as wave spectrum parameter extraction and a check of result's integrity.

The SSP developed for X-Band TS-X imagery (Pleskachevsky, Rosenthal, and Lehner, 2016) was extended for this study. The SSP contains optimized procedures for reading, calibration, filtering, subscene analysis including FFT and writing of results, including spectra and special point statistics. Hence, a rapid processing of thousands of S1 IW images as part of the model tuning process was possible. Figure 4 presents the current workflow of the extended SSP for TS-X and S1. The newly developed and extended blocks are marked by dark grey colour. Implemented into the processing chain of Ground Station in Neustrelitz allows SSP the processing and delivery of sea state products during 5–16 min after acquisition using actual hard- and software. This timing includes about 3–12 min data receiving, decoding and SAR image processing (level L0 and L1 processing) with following sea state processing with generation and delivery of wave products (L2 processing). The processing chain has been constantly improved, for more information on SSP and processing see Appendix 6.2.

2.4. *Artefacts pre-filtering and filtering surface signatures like spills and ship wakes*

A direct application of the EMF to a subscene often leads to inaccuracies in H_s with outliers in the range of meters (see 2.3). The sources of these errors are in the first place a number of natural and man-made artefacts like ships, large wind farm constructions, current boundaries, wind streaks and also atmospheric fronts. Even internal wave structures can impact the image spectra. Such spectral perturbations result in an

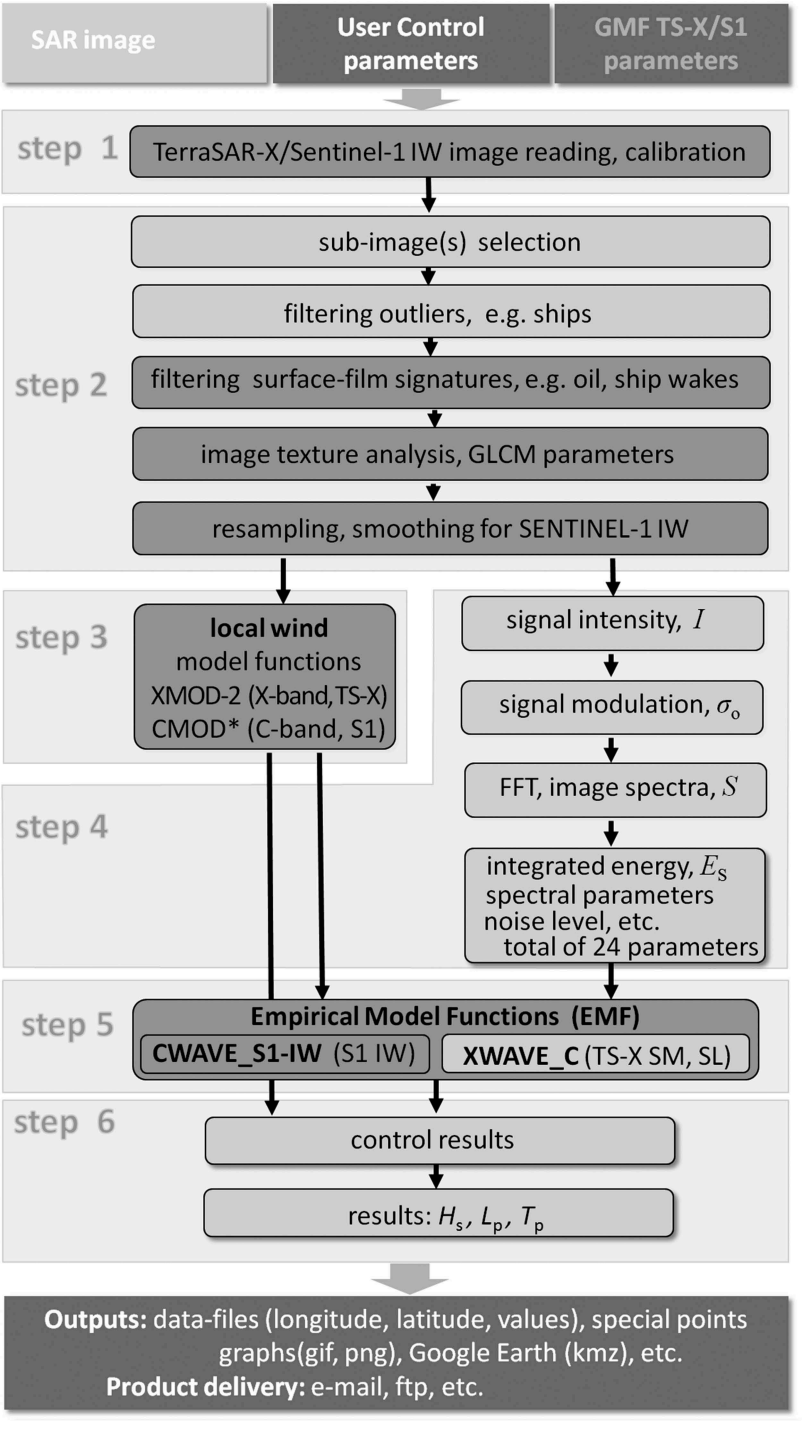

Figure 4. The Sea State Processor (SSP) for Sentinel-1 and TerraSAR-X. The SSP, initially developed for TerraSAR-X StripMap images with XWAVE_C function, was extended (dark grey boxes). The most significant extensions are the calculation of GLCM parameters, integration of CMOD5/CMOD4 wind function and including of the CWAVE_S1-IW sea state function. The current NRT version switches the processing for TerraSAR-X and Sentinel-1 images automatically.

integrated value which yields a contribution to the total energy not connected to the sea state. As shown in practice, the contaminating image artefacts can be divided into two classes:

(1) Radar echo much stronger than background backscatter from sea state, e.g. ships or offshore constructions like wind farms: a typical sea state overestimation for subscene with a ship of 10–120 m length without pre-filtering can amount ca. 2–15 m H_s. Filtering of such artefacts was already successfully implemented in SSP for TS-X imagery by using a simple but effective approach (Pleskachevsky, Rosenthal, and Lehner, 2016). After the statistics for a subscene are estimated based on $\langle\sigma_0\rangle$, the subscene is further analysed using a 100 m × 100 m (optionally) sliding window (sub-subscene). The statistics of each sub-subscene with a mean value σ_o^{sub} is compared with σ_o. In case of $\sigma_o^{sub} > q_{ship}\sigma_o$ with tuned coefficient q_{ship} = 2.30 (using 100 m × 100 m sub-subscene), the outlier pixels in the current sub-subscene are replaced by the mean value of the subscene's σ_o.
(2) Radar echo much weaker than background backscatter from sea state: such a situation can occur in the case of, e.g. ship wakes or oil spills. This phenomenon was encountered in the current study mostly when analyzing scenes in the Baltic. Such artefacts occurred at very high frequency in processing S1 data acquired during the summer algae bloom between Rügen Island and the Danish and Swedish coasts in the Arkona Sea (also ice structures occur during the winter). These structures together with ship wakes also led to an overestimation of the order of 1–3 m H_s. The filtering procedure of image contaminations was extended by employing $\sigma_o^{sub} < q_{spills}\sigma_o$ with tuned threshold coefficient q_{spills} (actually = 1.80 for 100 m × 100 m sub-subscene). Figure 5 shows an example of S1 IW acquired over eastern Baltic Sea and depicts artefacts of both kinds.

2.5. *Sentinel-1 IW images for sea state processor*

In comparison to TS-X StripMap with about 3 m resolution (pixel size of 1.25 m for spatially enhanced StripMap), the S1 IW resolution of about 40 m (pixel size of 10 m) is relatively coarse. A standard FFT window of 1024 × 1024 pixels covers an area of ca. 10,240 m × 10,240 m. The wave structures, if visible, are disturbed by noise and by the additional non-linear imaging of the waves. To get the swell structures more clearly, for the selected subscenes a resampling with a factor of four was applied. Each pixel is cut into 4 × 4 = 16 pixels with the same NRCS value but with a size of one-fourth of the original spacing. Then, a two-dimensional Gaussian smoothing was applied. After this procedure, the swell signals were significantly more stable with a prominent peak in the image spectra. The modified resolution amounts 2.5 m, the analysed FFT window (subscene) covers an area of 2560 m × 2560 m. Figure 6 shows an example for a subscene before and after resampling and smoothing. The tuning of the complete dataset of ca. 800 collocations in the North Sea with and without resampling/smoothing shows significant improvement of about 30 cm RMSE in the case that the procedure is applied (see further in 2.7). The scatterplots of algorithm tuning point out the stronger scattering for original data and lower accuracy.

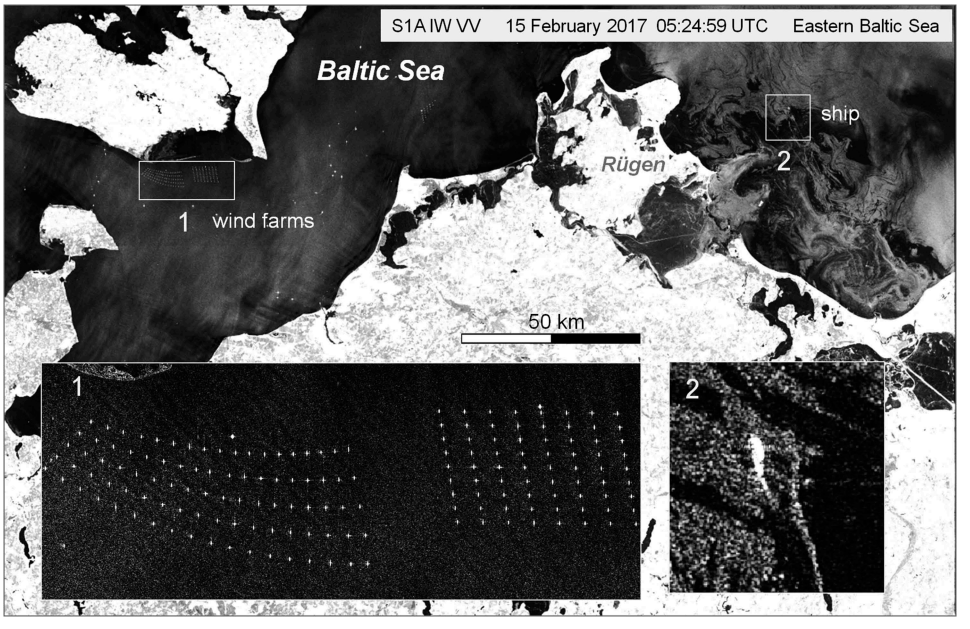

Figure 5. Sentinel-1 IWscene in VV pol. acquired over Eastern Baltic Sea on 15 February 2017. Artefacts of both kinds are present: very high radar echo from ships and weak radar echo by surface slicks. The edges of such films produce also an entry of spectrum energy. Relatively narrow slicks like ship wakes can be misinterpreted as a long surface wave.

2.6. *Parameter used for tuning the model function*

The CWAVE_S1-IW approach was initially validated for the North Sea (about 30 buoys). Later, collocations were extended to the North Atlantic and Baltic Sea and then the west and east coasts of USA and Canada, the Aleutian Islands and Hawaii followed. All scenes were pre-processed, and the primary parameters estimated by subscene analysis were collected (for detailed information and examples, see Appendix Table A1). A series of secondary parameters derived from the primary parameters like rates between different kinds of spectrum energy and noise in different spectral domains were also estimated.

For obtaining integrated wave parameters, a Fast Fourier Transform (FFT) operation was applied to the radiometrically calibrated and normalised subscenes with a size of 1024 × 1024 pixels (see eq.1, eq.2). The resulting image power spectrum $S(k_x,k_y)$ is the basis for estimating the sea state parameters. The integrated energy E_S is defined by the following formula describing a common integration of a 2-D area in terms of the wavenumber coordinates:

$$E_S = \int_{k_x^{min}}^{k_x^{max}} \int_{k_y^{min}}^{k_y^{max}} S(k_x,k_y)\,dk_y\,dk_x \tag{4}$$

where $S(k_x,k_y)$ results from FFT analysis of a landmasked, normalised and pre-filtered 2.5 km × 2.5 km subscene. The land masking is connected to the algorithm for coastal line estimation from the same scene (Wiehle, and Lehner, 2015). The threshold for

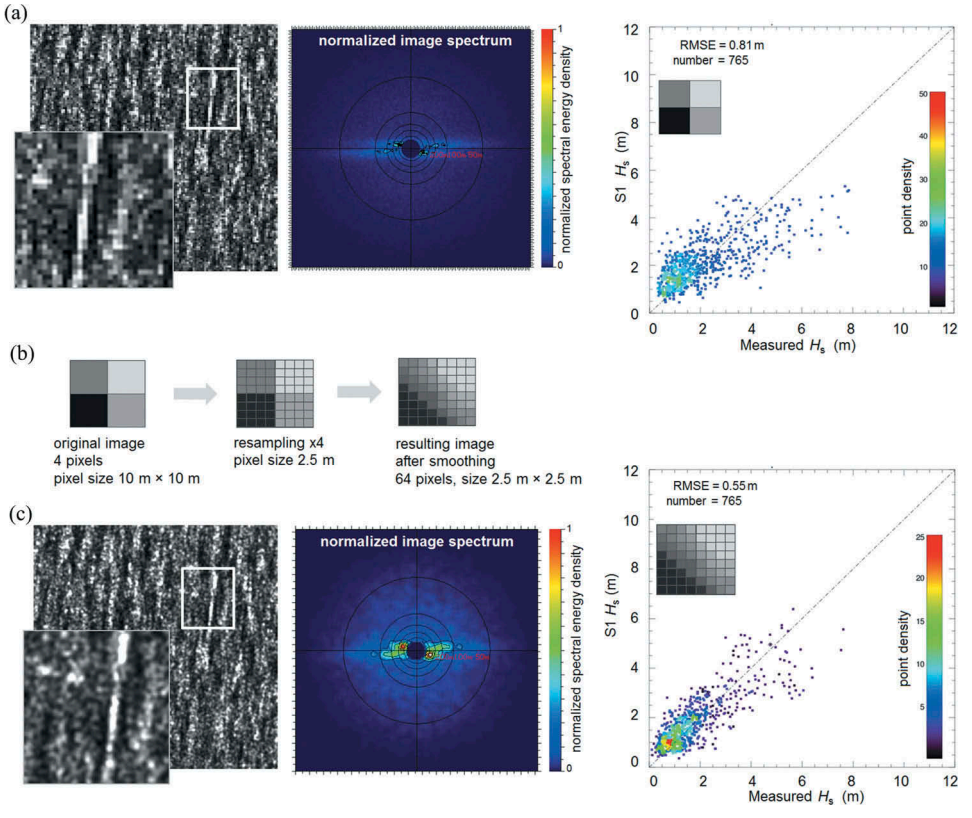

Figure 6. Effect of resampling and smoothing of original Sentinel-1 IW data. (a) An example of subscene 2.5 km × 2.5 km, corresponding normalised image spectrum and tuning results for the North Sea by original data and (c) after applying resampling and smoothing. (b) An example of transformations for four original pixels. The RMSE improves by 30 cm when smoothing is applied, and the same EMF is used. The point density colour bar represents an account of H_s in boxes ±20 cm around actual H_s value.

switching a subscene between active/inactive (land) is 20% of the land pixels in a subscene (Rikka, et al. 2018b. and also this study). To avoid signals from land structures and especially from the water-land border (very problematic in the Baltic Sea where dozens of small rocks can appear in a subscene and result in a strong false alarm signal) the land pixels are replaced by $\langle\sigma_0\rangle$ calculated using water pixels only.

The integration domain for E_S is limited by $k_x^{max} = k_y^{max} = k^{max} = 0.201$ and $k_x^{min} = k_y^{min} = k^{min} = 0.003$ with k^{min} corresponds to maximum considered wavelength $L_{max} = 2000$ m and k^{max} corresponds to minimum wavelength $L_{min} = 30$ m, where wavenumber $k = (k_x^2 + k_y^2)^{\circ.5}$. The integration interval was specified for the following reasons: S reflects the image spectrum energy corresponding to the sea state: in image spectra results from S1 IW, the domain ca. $0.060 < k < 0.200$ represents the radar clutter, produced by waves shorter than ca. 100 m wavelength, the domain ca. $0.010 < k < 0.060$ represents the long waves with wavelength ca. 100 m $< L_p <$600 m, and the domain ca. $0.003 < k < 0.010$ represents even longer structures like so-called wind streaks. These streak structures with lengths of ca. 300–1200 m on the sea surface are

produced by airflow turbulent eddies at boundary layer (Etling, and Brown, 1993). Itegration for these domains results in partial energies E_S^{100}, E_S^{600}, E_S^{2500} (see Table A1 in Appendix).

The nonlinearity of wave SAR imaging makes difficult to distinguish the sea state by using only spectral analysis in case of S1 IW (see Figure 2). For example, in the case of strong winds with local wind sea higher than 2–3 m (especially by wave breaking), the underlying swell can be practically hidden by noise and streaks produced by wind sea waves. In this case, swell waves do not produce an appropriate peak in the image spectrum. To improve the accuracy of sea state estimation for all weather conditions, additional information was considered using image texture feature analysis (GLCM).

GLCM is a tabulation of the frequency of different combinations of pixel brightness values occurring with certain distances in certain directions to each other in an image. The idea of using GLCM image analysis for oceanography applications is not new and widely used for ice coverage classification (e.g. Ressel, Frost, and Lehner, 2015) and oil detection (e.g. Singha, Vespe, and Trieschmann, 2013). For this study, the eight basic GLCM parameters are estimated and used for tuning: GLCM-mean, variance, correlation, entropy, homogeneity, energy, contrast and dissimilarity. The GLCM matrix is calculated for each subscene from the original IW data before resampling and smoothing (see Appendix Eq. A1–Eq. A8).

A comparison of all eight estimated GLCM parameters (see Table A2) with collocated sea state measurement revealed that the homogeneity is more definitely connected to the H_s than other GLCM parameters. The GLCM-homogeneity measures the uniformity of the non-zero entries in the GLCM matrix: if the image has little variation then homogeneity is high, and it equals one for a constant image. Figure 7 presents the relationship between GLCM-homogeneity and measured H_s acquired over the North Sea. From

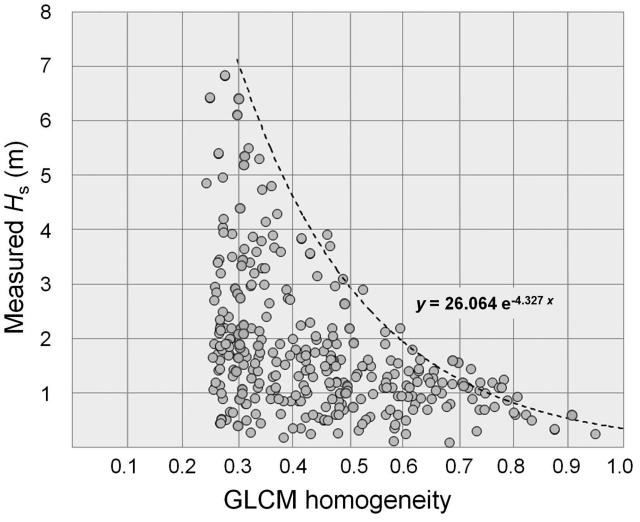

Figure 7. Local GLCM-homogeneity for collocated subscenes and sea state measurement in the North Sea (L_p under 250 m). The damping effect of higher waves is clearly visible in homogeneity. The enveloping line was approximated and applied as a filter for local maximal wave height.

the graph, an enveloped function was designed describing the dependency of the observed max H_s on homogeneity estimated from collocated S1 IW subscenes. This tuned function was applied as a filter (threshold) for the maximal wave height H_s^{max} using a simple empirical exponential approximation:

$$H_s^{max} = x_1 e^{\,x_2 C_{homogeneity}} \tag{5}$$

where $C_{homogeneity}$ means GLCM-homogeneity (see Appendix Eq. A4), x_1 = 26.064 and x_2 = −4.327. This filter includes all measurements in the North Sea with L_p up to ca. 250 m (peak period of ca. 12 sec). All North Sea storms acquired in 2014–2016 by S1 are accompanied by strong local winds and do not include the situations of high and long swell waves with H_s> ca. 3 m, propagation L_p > 200 m (E_S^{600} > ca. 0.111) and under calm weather conditions (U_{10} < 8.0 m s^{-1}), which can be observed in the open Atlantic.

The next finding was the correlation between a systematic underestimation in H_s based only on spectral analysis and local wind speed on the order of 0.5 m with GLCM-entropy under calm weather conditions (GLCM-entropy is a measure of spatial disorder; a completely random distribution would have very high entropy). Under the same wind speed but with larger fetch the wind sea waves are higher and produce noise in the SAR image resulting in differences in entropy. The spectral analysis and wind speed itself do not give enough unambiguous information to distinguish these conditions. A correction for low sea state for GLCM-entropy <2.0 was included into the EMF (see 2.5 and Figures A1 and A2).

2.7. Resulting algorithm function

The CWAVE_S1-IW EMF is based on the direct estimation of integrated sea state parameters from SAR image spectra without transformation into wave spectra. CWAVE_S1-IW was tuned according to collocated buoy data and wave models results.

The CWAVE_S1-IW EMF for S1 IW images calculates the H_s by the following equation:

$$H_s^{CWAVE\_S1-IW} = a_1 \sqrt{B_1 E_S \tan\theta} + \sum_{i=2}^{n} a_i\, B_i \tag{6}$$

where a_i are tuned coefficients, and B_i are correction functions described as follows: B_i are based on spectral parameters, on local surface wind U_{10} estimated using CMOD-5 for VV Hersbach, 2003) and CMOD-4 for HH pol. algorithms (Hersbach, Stoffelen, and de Haan, 2007) and on GLCM parameters. n = 5 defines the current number of corrections. The corrections have been extended in cases of new situations (e.g. hurricane Irma) not considered before when new data are acquired. The CWAVE_S1-IW EMF has the same form as the XWAVE_C function developed for TS-X SM processing (Pleskachevsky, Rosenthal, and Lehner, 2016). However, the corrections and coefficients have another meaning and are based on other parameters.

The square-root term $a_1 \sqrt{B_1 E_S \tan\theta}$ represents the general connection between sea state and energy in image spectra. It contributes mostly in case of long prominent imaged waves with wavelength exceeds 100 m. Based on the definition of significant wave height estimation from wave spectra energy E_{WS}, $H_s = 4\sqrt{E_{WS}}$, a_1 = 4.0 and B_1 is scaling of image spectrum energy E_S concerns the character of non-linearity of the SAR-imaging mechanism of ocean waves. $B_1 = K_1 \times E_S^{100}/E_S^{600}$ is a relation between E_S^{100} integrated with the 30–100 m

wavelength domain (only noise falls into this spectral domain for S1 IW images) and E_S^{600} in the spectral ring with 100–600 m wavelength, where wave-like patterns produce the peak (integration see eq.4, more details in Appendix). The constant K_1 = 17.015 is tuned using collocated buoy data.

The summation term with i = 2–5 presents a series of corrections of different origins. The term a_2B_2 represents local wind impact/offset with$B_2 = U_{10}$. The local surface wind speed is estimated using CMOD-4/CMOD-5 algorithms. a_2 = 0.11 is defined for U_{10} < 16 m s^{-1}. However, for winds exceed 16 m s^{-1} and especially for directions near to the sensor flight direction, an additional correction is needed. Note, an identical outcome was also found for X-band TS-X imagery (Pleskachevsky, Rosenthal, and Lehner, 2016): for strong wind U_{10} > 18 m s^{-1} (Beaufort 9) due to the transition of the wave regime into strong breaking and flying water particle targets the SAR-imaging also changes. The wave breaking effect, in particular, complicates the estimation in case of waves breaking into the SAR flight direction. This direction can be different from the direction of swell propagation in the case of two wave systems under strong wind conditions.

The term a_3B_3 represents the correction for clutter produced by wind sea under similar wind conditions but with a different fetch (see 2.6). For GLCM-entropy <2.0, the a_3 = 1.21, $B_3 = (C_{entrophy}1.1)^{5.5}+0.44$ are tuned using *in-situ* measurements with contributions to H_s in the range of 0 m to ca. 1.5 m. The identical background has the term a_4B_4 by using GLCM-dissimilarity. $B_4 = C_{dissimilarity}$ and a_4 = 0.11. $a_5B_5 = -1.8$ is a common tuned model function offset.

2.8. *Algorithm tuning*

The EMF has been tuned by minimisation of RMSE for collocated H_s measurements. The tuning began by two basic function components: the first square-root term represents long wave's presence, and the term a_2B_2 represents local wind influence. For the establishment of a full appropriate *ansatz-function* (Karbach, and Müller, 1997) for Eq.6 that is capable of representing all significant phenomena, the correlation of the errors with the parameters (see Appendix Tables A1 and A2) was studied and parameters which mostly affect the accuracy were selected.

Firstly, a weighting function B_1 was designed for long swell waves under very low wind conditions; further, the weighting factor a_2 was tuned using different wind conditions. The next step was to study short sea state by a series of correction terms, which are based on spectral and GLCM features used to compensate for outlier-errors of different origins. To minimize the RMSE, the pairwise differences of the two data sets were analysed: S1 IW estimated values and collocated measured values:

$$\mathrm{RMSE} = \sqrt{\frac{1}{N}\sum_{j=1}^{N}\left(H_{s_j}^{S1} H_{s_j}^{buoy}\right)^2} \tag{7}$$

where $H_{s_j}^{S1}$ represents wave height estimated using Equation.6 and Equation.5, $H_{s_j}^{buoy}$ is the corresponding collocated *in-situ* H_s for collocation pair j with N defining the total number of all collocated samples of all buoys (see 2.2 and Table 1).

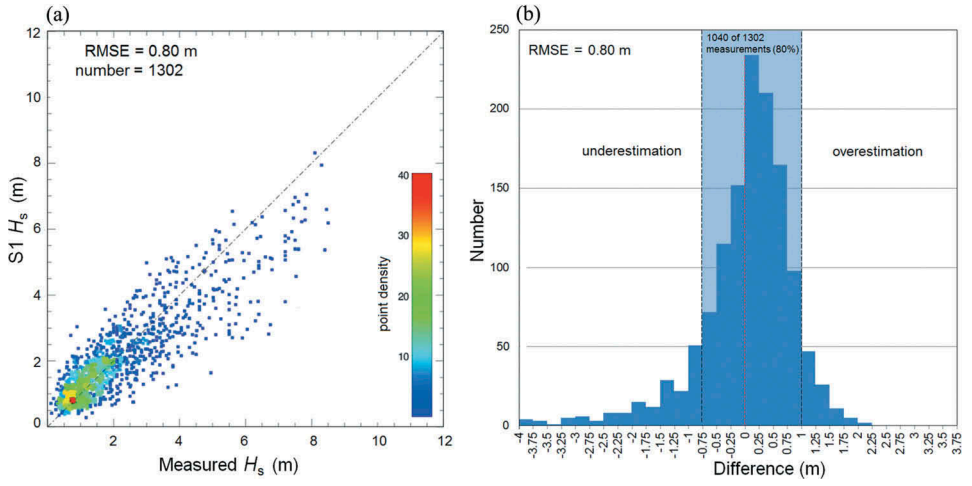

Figure 8. (a) Results for tuning of the EMF Eq.6 and Eq.5 worldwide performed by using S1 IW data acquired in 2014–2015 with RMSE = 0.80 m. For the tuning, all collocated subscenes were automatically extracted and analysed (no manual exclusion of data), also for huge storms with H_s > 6 m. For the H_s < 5 m RMSE = 0.61 cm. (b) A histogram displays a distribution of the underestimations and overestimations (right). The vertical red line shows the '0' error to measurement. The absolute differences between measurement and estimated H_s are presented by a binning of 25 cm; the variation ±25 cm against the measurements consists of 34%, ±75 cm consists of 55% of all cases.

The algorithm was developed for practical NRT services where data must be processed for a wide spectrum of environmental conditions. Thus, the focus of the EMF's establishment and tuning was robustness, simplicity and performance. Figure 8 shows the tuning of the EMF worldwide performed using S1 IW data acquired in 2014–2015 with resulting RMSE = 0.80 m. For the tuning, all collocated subscenes (defined in section 2.2) were automatically extracted and analysed, including huge storms with H_s > 8 m. For H_s < 5 m the RMSE achieved was 0.61 cm. The histogram displays a distribution of the underestimations and overestimations of the algorithm (Figure 8, right). The vertical red line marks perfect agreement. The absolute differences between measured and estimated H_s are presented in bins of 25 cm; the ranges ±25 cm and ±75 cm contain 34% and 55% of all cases, respectively.

3. Validation

This section presents the validation results together with some examples of processed scenes and test cases.

3.1. *Validation*

For validation of the algorithm and the SSP, S1 IW images acquired in 2016–2017 were used (see 2.2 and Table 1). The validation dataset contains almost all of the images acquired in the south-east North Sea and western Baltic Sea. Since 1 January 2017, an automatic NRT processing for all S1 IW in this region has been running. The sea state in

the range of 0–5 m H_s with mean value H_s^{mean} of 1.2 m was acquired. Additionally, most of the North Atlantic storm S1 IW data were selected and included (H_s range 3–11 m, $H_s^{mean} \approx 6.1$ m). The validation RMSE amounts to 0.62 m and is better than 0.80 m, which was obtained during tuning (see Figure 9). After scene-by-scene analysis, the better performance during validation can be explained by the larger underestimations for $H_s >$ 5 m in the tuning data set (see in Figure 8) owing to the specific nature of the storms acquired. These storms in 2015 include strong winds above 15 m s^{-1} mostly blowing close to the SAR flight direction.

A more detailed study showed that for different sea state domains, the accuracy is different. This accuracy difference exists due to the differences in SAR imaging for the different kinds of sea state dominating in different regions. Table 2 presents accuracies for different sea states ordered by H_s. Although the RMSE deteriorates with increasing H_s (0.30 cm for mean $H_s \approx 1$ m and 1.20 m for mean $H_s \approx 6$ m), the scatter index (SI, RMSE normalized by the mean value of the measurements, shown in the last line of the table) improves for higher sea state (30% for mean $H_s \approx 1$ m and 20% for mean $H_s \approx 6$ m).

3.2. *Strom acquisitions with high variability in wind and wave fields*

An additional factor influencing the accuracy is the variability in the fields under storm conditions: wind gusts and corresponding clusters of increased waves. The local impact of these gusts on ocean waves can increase significantly if the speed of the gust propagation is close to the speed of the wave groups. Wind energy feeding the same wave group for a longer time period causes a growth of individual waves and results in resonance. The earlier studies using SAR data (C-Band ENVISAT ASAR) have already shown that wave groups with abnormal height in the North Sea are connected to atmospheric effects (Pleskachevsky, Lehner, and Rosenthal, 2012). It turned out that they are caused by mesoscale wind gust cells with a size of around 50 km that are moving as an organized system across the sea and 'drag' the continuously growing waves. An identical effect on a smaller scale was also observed in the North Sea and in the Baltics using high-resolution TS-X (X-band) SAR data. Clusters with a size of only a few kilometres with local wind gusts show a local sea state variability with H_s increase of 1 m to 2 m (Rikka, et al. 2018a).

Under storm conditions, this variance can influence the resulting analysis. In fact, a buoy represents the statistics of a relatively small sector of sea state propagating towards the buoy, integrated over time (typically a 20-min time series). S1 IW data represent H_s from subscene statistics of a wider snapshot, which can illustrate the spatial variability. Figure 10 shows an example of a sequence of 12 S1 IW images acquired over the North Atlantic on 4 January 2016 under storm conditions with H_s reaching 9 m and covering an area of approximately 250 km × 2200 km. For the image N5 the sea state

Table 2. Accuracies of wave height estimation for different ranges of H_s includes wind sea and swell.

	H_s interval (m)		
Parameter	$0 < H_s < 2$	$2 < H_s < 4.5$	$4.5 < H_s$
RMSE (m)	0.30	0.62	1.23
SI	0.31	0.19	0.20
H_s^{mean} (m)	1.03	3.26	6.02

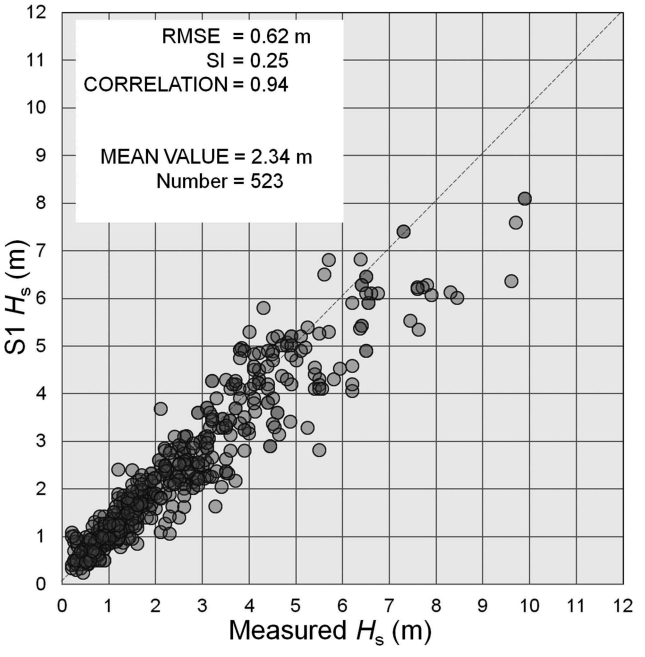

Figure 9. Validation of the sea state processor carried out in the North Atlantic including the North Sea and western Baltic Sea.

estimation is shown processed with a raster of 3 km. The variability around the measurement station 64,045 (EMODnet, 59.100N −11.401W) is very high. Under the gust cells with increased wind speed, the sea state grows up to 8 m, with a mean H_s value of around 6 m. Comparisons with the six measurements and the WWIII wave model results are shown.

4. Test cases and NRT application

This section demonstrates the application of the method under various conditions in different regions worldwide. An example of storm tracking from the point of view of MSA is shown. Also, a first application for supporting a research ship cruise in the Antarctic Sea is discussed.

4.1. *Sea state in different regions*

During testing of the performance of the method and the SSP, acquisitions for different conditions in different areas were processed and compared with forecast model results and *in-situ* measurements: Hawaii, the west and east coasts of USA and Canada, the Aleutian Islands, Australian coasts, the Persian Gulf, Atlantic, North Sea, Baltics, and Black Sea. The significance of these investigations was the proof that the algorithm is stable, working with the various wave systems that dominate in different regions with differences in SAR imaging. For example, for a H_s of ca. 5 m in the North Sea during a storm typically at least 30% of the amplitude comes from the swell component with L_p over

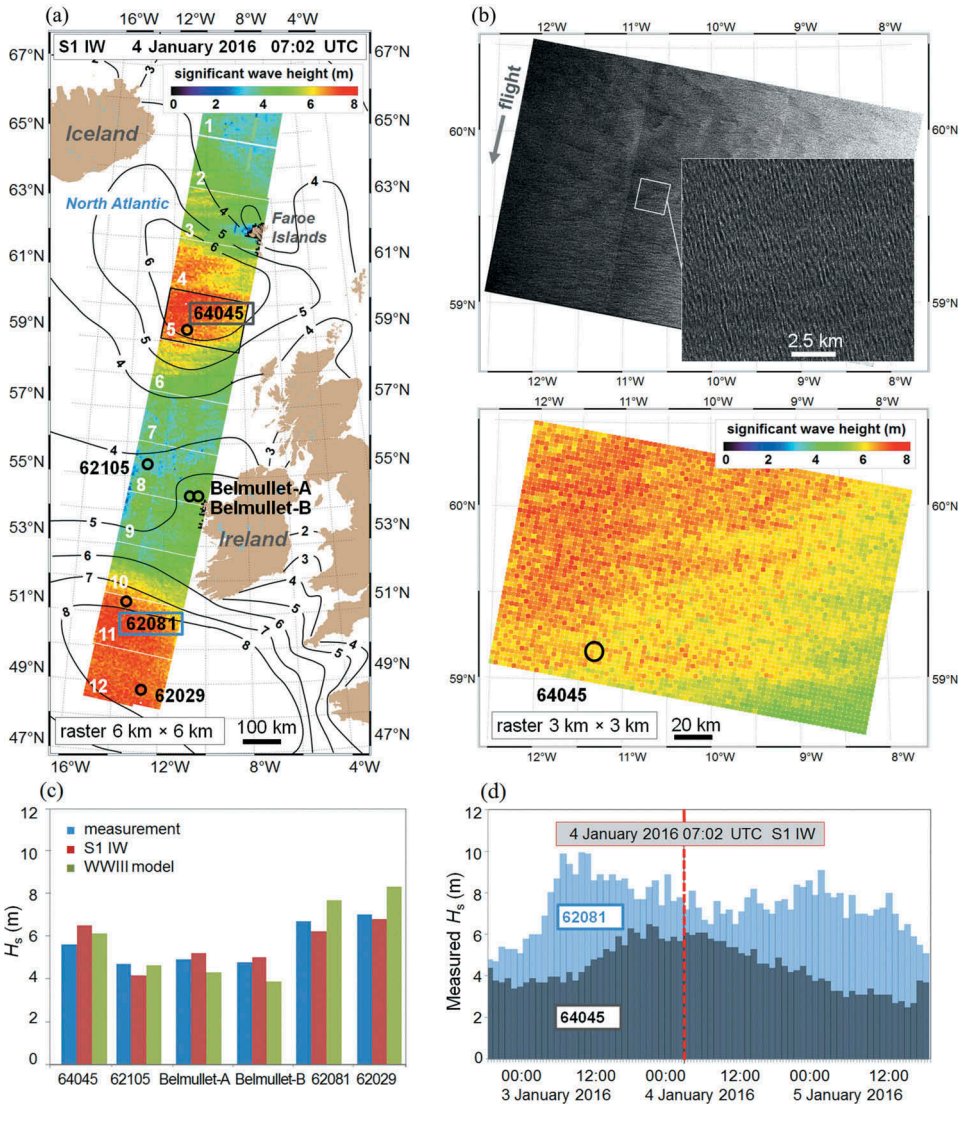

Figure 10. (a) An example of a sequence of 12 S1 IW images acquired over North Atlantic under storm conditions with H_s reaching ca. 9 m and covering an area of approximately 250 km × 2200 km processed with a raster of 6 km (30 × 40 = 1200 subscenes per image). Isolines represent the forecast model WWIII of NOAA and circles are measurement stations (EMODnet). (b) S1 IW image N5 and sea state processed with a raster of 3 km for this image. The variability around measurement station 64,045 is very high: under the gust cells with increased wind speed the H_s in wave groups grow up to 8 m by a mean value of ca. 6 m H_s. (c) Comparison with measurement and wave model for collocated measurement stations. (d) Time series for two measurement stations 64,045 and 62,081 shows the variability and rapid changing of local H_s.

250 m coming from the North Atlantic. The same H_s of ca. 5 m in the Baltics and in the Black Sea is more exclusively dependent upon the local sea state, with shorter steeper waves under fast-moving cyclones. In the following sections, examples of individual cases for storms in the Black Sea will be shown.

4.2. *Test case: storm tracking in the black sea*

In the Black Sea, the averaged H_s is about 1.2 m and the sea state allows ship traffic of all kinds. The storms here develop fast and cannot be foreseen like in the North Sea, where storms usually develop first in the Atlantic over a period of days and later move into the North Sea.

In Figure 11 a case of storm tracking in the Black Sea in April 2017 during three days is shown with six S1 IW acquisitions using the technique developed in this study. The storm peak estimated from S1 acts similar to the predicted storm moving across the Black Sea. However, despite the similarity in H_s, spatial distribution and propagation, the observed peak is shifted around 80 km to the south in comparison to the model forecast simulations running by Institute of Coastal Research at the Helmholtz-Zentrum Geesthacht, Germany (HZG, n.d.). During this storm, a cargo ship 'Geroi Arsenala' was capsized about 40 km to the south of the Kerch Strait. The ship of the river-sea class

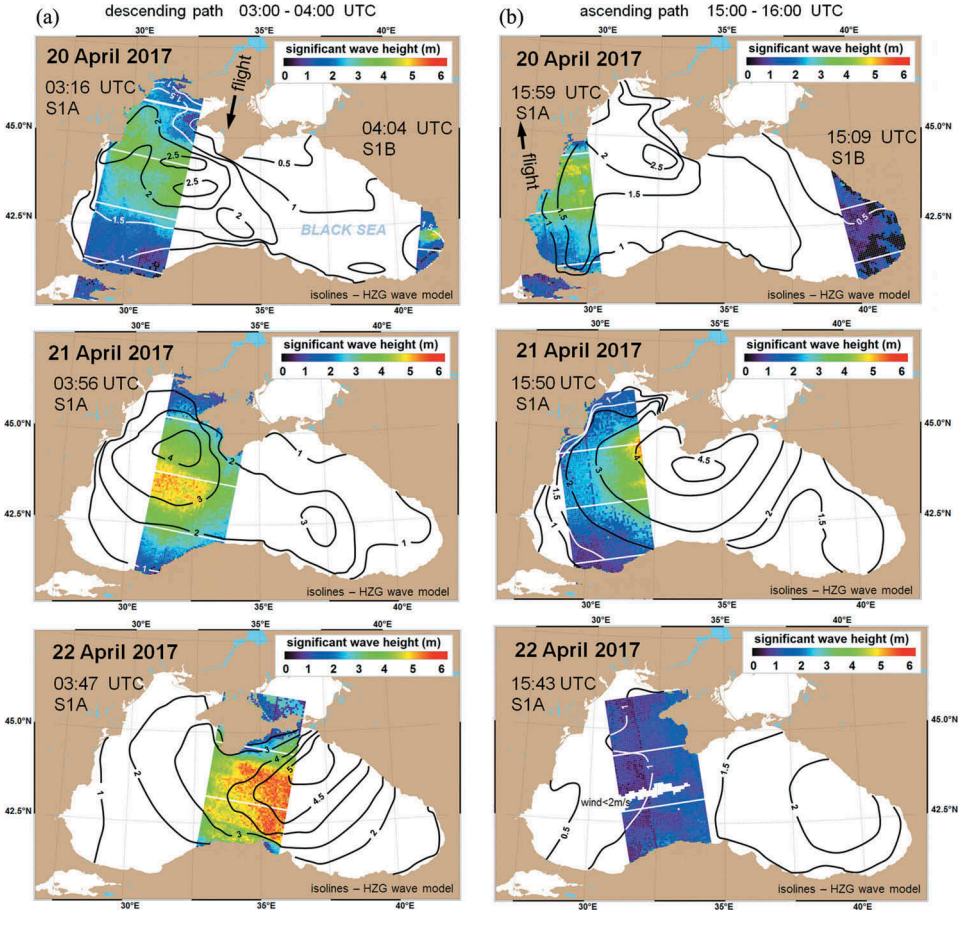

Figure 11. Estimated sea state in the Black Sea. A storm in April 2017 is tracked over three days. (a) S1-A and S1-B descending and (b) ascending path. The isolines show the results of the forecast numerical wave model developed and run by HZG. The storm peak estimated from S1 has shifted 80 km to the south in comparison to the model simulations (21 April 2017 at 03:56 UTC, descending pass).

(intended for large inland waterways with access to the sea with H_s not exceeding 2 m and not farther than 20 km from the sea coast) was carrying grain from Russia to Turkey. Only one of the 12 people aboard were rescued according to the Associated Press. Obviously, the course was taken too far from the coast to shorten the way across the sea with unexpected high sea state. Using the new methods and remote sensing information will help to avoid such situations.

4.3. *Supporting of a scientific cruise in Antarctic ocean*

The first validation of the algorithm and processor under real conditions were carried out during a scientific cruise in the Antarctic Sea with NRT delivery of the estimated wave fields to the crew onboard.

Navigation in Antarctic waters is challenging. Drifted by wind and currents, the sea ice situation can change significantly within hours. A validation of the wind and sea state forecast (used for ship navigation) with *in-situ* buoy measurements in most cases is excluded. The remote sensing measurements are only available to verify the forecast model results (e.g. WWIII NOAA).

In order to gain interdisciplinary knowledge, the Antarctic Circumnavigation Expedition (December 2016 to March 2017) brought together scientific teams from different countries on board the Russian research vessel 'Akademik Treshnikov' for a 3-month journey around the Antarctic continent, providing circumpolar measurements of many marine variables (Frost, et al. 2018). The German Aerospace Center (DLR) supported this campaign with SAR acquisitions downlinked and processed in NRT at the DLR ground segment in Neustrelitz. SAR quicklooks and L2 products, namely operational H_s retrieval and sea ice classification, were delivered automatically within 20 min after downlink. Figure 12 presents an example of H_s estimation for the Heard and McDonalds Islands in the Antarctic Ocean under storm conditions with H_s about 3–5 m, acquired on 5 January 2017 using S1 IW. The *in-situ* measurements are not available for this area; the isolines show the H_s from WWIII model results for 5 January 2017 at 14:00 UTC. The red marked image was processed and delivered in NRT directly onboard the research vessel 'Akademik Tryoshnikov'.

4.4. *Monitoring in the North Sea and the Baltic using sentinel-1 IW*

From the point of view of monitoring, the most common question is how often it is possible to get the information for S1 IW for a given geographic location (e.g. a buoy). In the case of the North Sea and the Baltic, S1 IW are taken daily, twice by ascending (between ca. 15:40 UTC in the Gulf of Finland and 17:30 UTC in the English Channel) and descending (between ca. 04:00 UTC in the Gulf of Finland and 06:20 UTC in the English Channel) overflights. However, each acquisition-strip taken the next day is shifted by ca. 100 km to the east for geographic latitude between ca. 50°N and 60°N (see Figure 13).

Due to this shifting, only 10–12 acquisitions are practically possible by S1 IW, taken directly over a location during one month (although more than a dozen acquisitions were usually taken around a selected geographic location). Figure 14 shows an example of S1 IW acquisitions taken around wave rider buoy 'Sylt' in German Bight of the North Sea located about 10 km from the shore in February 2018. More than 60 acquisitions in

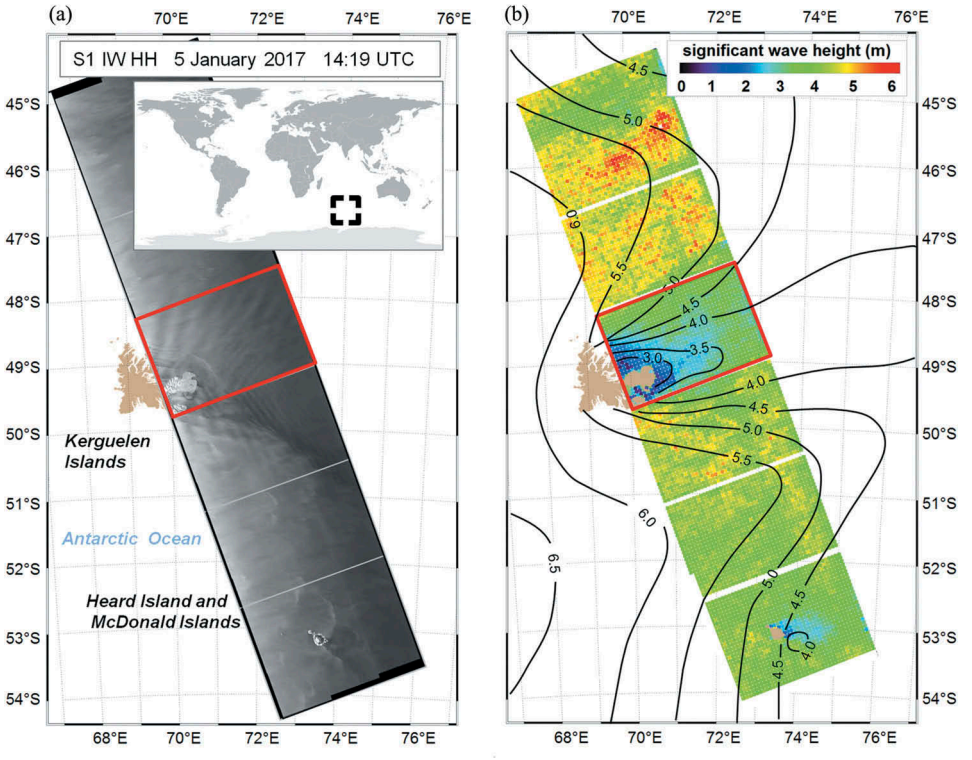

Figure 12. An example of wave height estimation in the Antarctic Ocean under storm conditions with H_s about 3–5 m acquired on 5 January 2017. (a) S1 scene and (b) estimated H_s. Direct measurements are not available; the isolines show the H_s from WWIII model results. The red marked image was proceeded in NRT and delivered directly onboard the research vessel 'Akademik Tryoshnikov.'

the area have been taken during the month; the buoy location was directly acquired 12 times due to satellite orbit shifting.

5. Discussion and outlook

This section summarizes the theoretical conclusions gained in the study related to algorithm development and to sea state SAR imaging. The technical realization of the algorithm is also discussed.

5.1. *Sea state in sentinel-1 IW images and sea state function*

The examination of S1 IW images shows that the imaged sea state can be divided into three classes with different SAR imaging, requiring separate consideration: very short wind sea imaged as noise (1), long waves with L_p> ca. 120 m imaged as a wave pattern under moderate wind condition (2), and strong storms with wind speed U_{10} > ca. 15–18 m s^{-1} and wave amplitude >4–5 m with wave breaking effects covering the wave pattern (3).

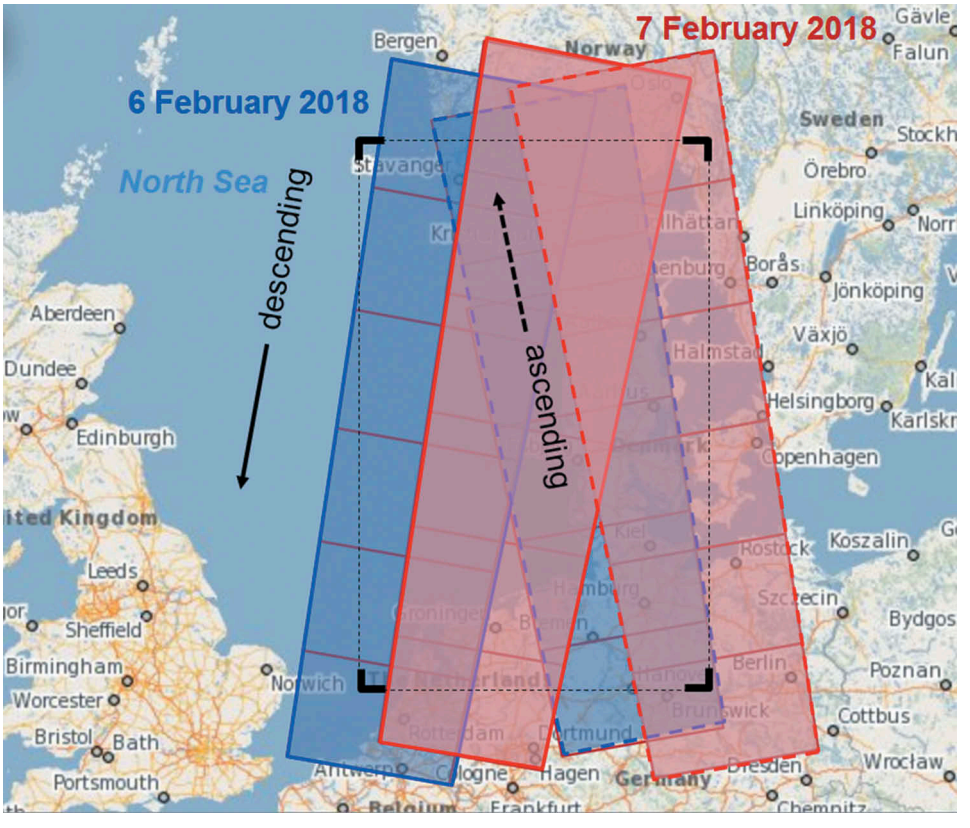

Figure 13. An example of Sentinel-1 IW acquisitions in the North Sea (touched marked area) during 2 days: 6 January 2018 (blue) and 7 January 2018 (red) with descending orbit ca. 06:00 UTC and ascending orbit ca. 17:00 UTC. The acquisitions are shifted at ca. 100 km to east every next day; repetition appears with 6-day cycles (11 days for each S1A and S1B).

The CWAVE_S1-IW EMF for estimation of meteo-marine parameters from C-band SAR data was developed for taking into account different sea states with different SAR imaging mechanisms. It was found that the parameters of short waves with no visible imaged wave pattern can be estimated based on a combination of local wind information, the properties of image spectrum noise and GLCM parameters, where the GLCM-homogeneity and GLCM-entropy features are the most suitable.

The validations show that the underestimation observed for waves larger than ca. 5 m are connected to local winds blowing into the near-azimuth direction with speeds exceeding 15–17 m s^{-1} (Beaufort-7 and more) that lead to SAR imaging effects from wave breaking. An automatic correction for these cases is currently under development. It was also found that changes in the wave regime caused by wind speeds ca. U_{10} > 18 m s^{-1} (transferring into intensive wave breaking, Beaufort 9) lead to superimposition of the wave imaging with strong noise, which conceals the wave pattern in the SAR images.

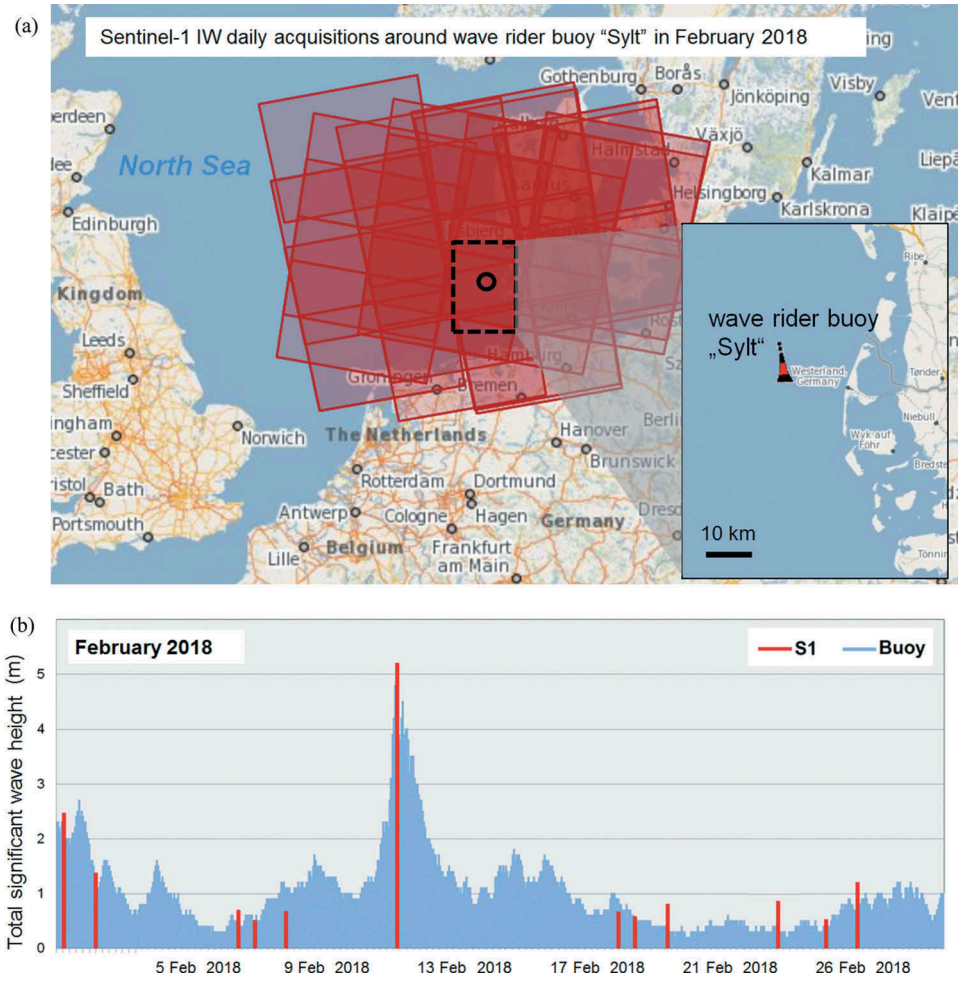

Figure 14. (a) Daily S1 IW acquisition around wave rider 'Sylt' in German Bight of the North Sea in February 2018. (b) the measurement time series (blue) and S1 IW estimated (red) wave height for February 2018. More than 60 acquisitions in the area have been taken during the month; the buoy location was directly acquired 12 times due to satellite orbit shifting (offset).

5.2. *Sea state processor for practical and operational use*

The CWAVE_S1-IW was incorporated into the operational NRT version of the SSP initially developed for the TS-X and TanDEM-X (TD-X) satellites (Pleskachevsky, Rosenthal, and Lehner, 2016, Schwarz, et al. 2015, Pleskachevsky, et al. 2017). For MSA, the image can be processed into different information layers (surface wind, sea state, ship detection, etc.). Figure 15 shows an overview of the concept developed at DLR and realized in a prototype version for NRT service validation at DLR's Ground Station in Neustrelitz. The service runs daily for the Southern North Sea and Western Baltics on S1 IW imagery since February 2017 and the current configuration provides sea state and wind parameters on 6 km × 6 km geo-coded raster.

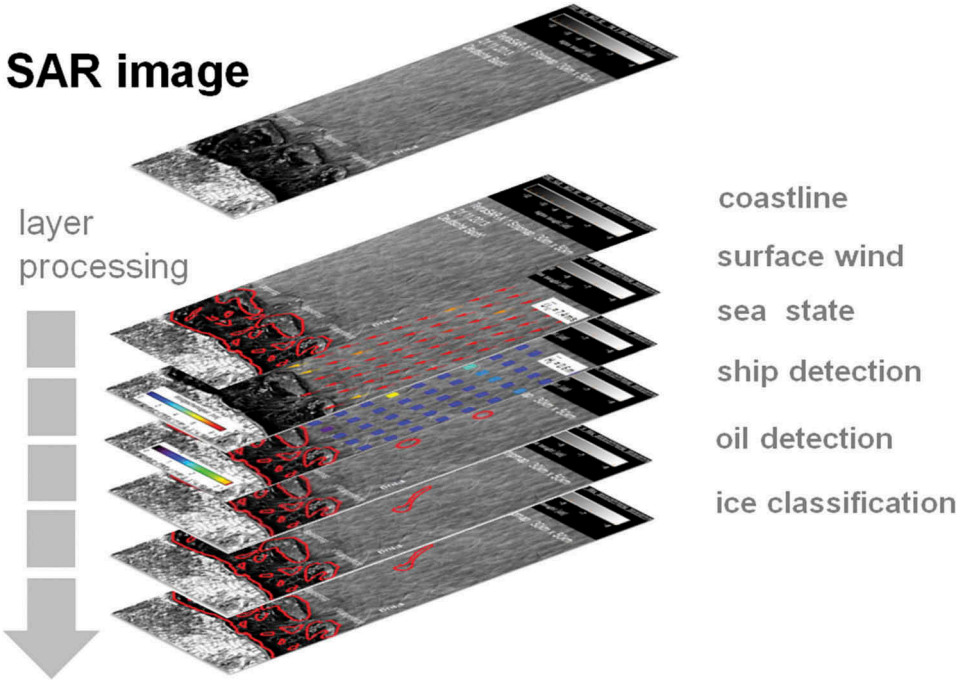

Figure 15. Processing of a SAR image for maritime situation awareness. Information from different layers is shared with each other to improve product accuracy.

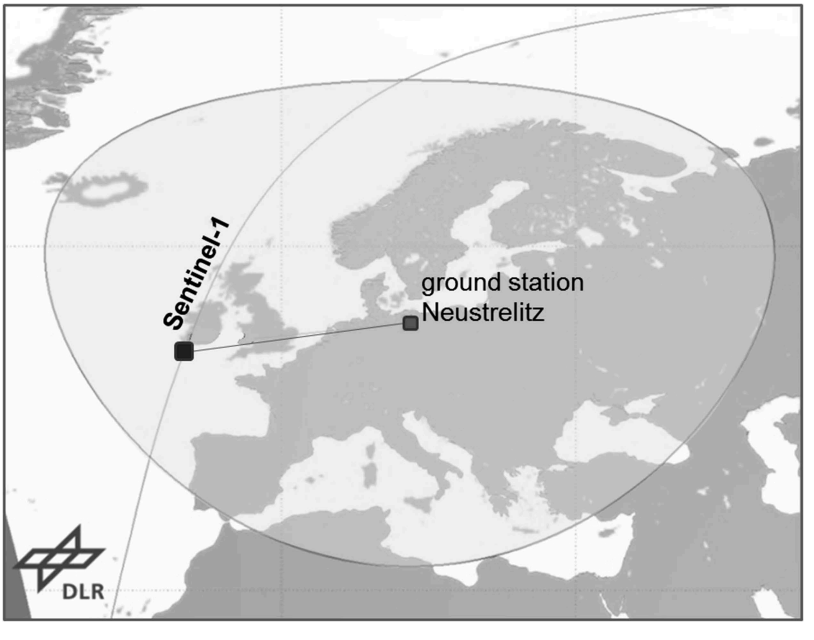

Figure 16. Ground Station Neustrelitz, acquisition circle for Sentinel-1, 5° elevation. Inside of this area, the data can be transferred from satellites to ground station directly after the acquisition, without delay, for NRT processing.

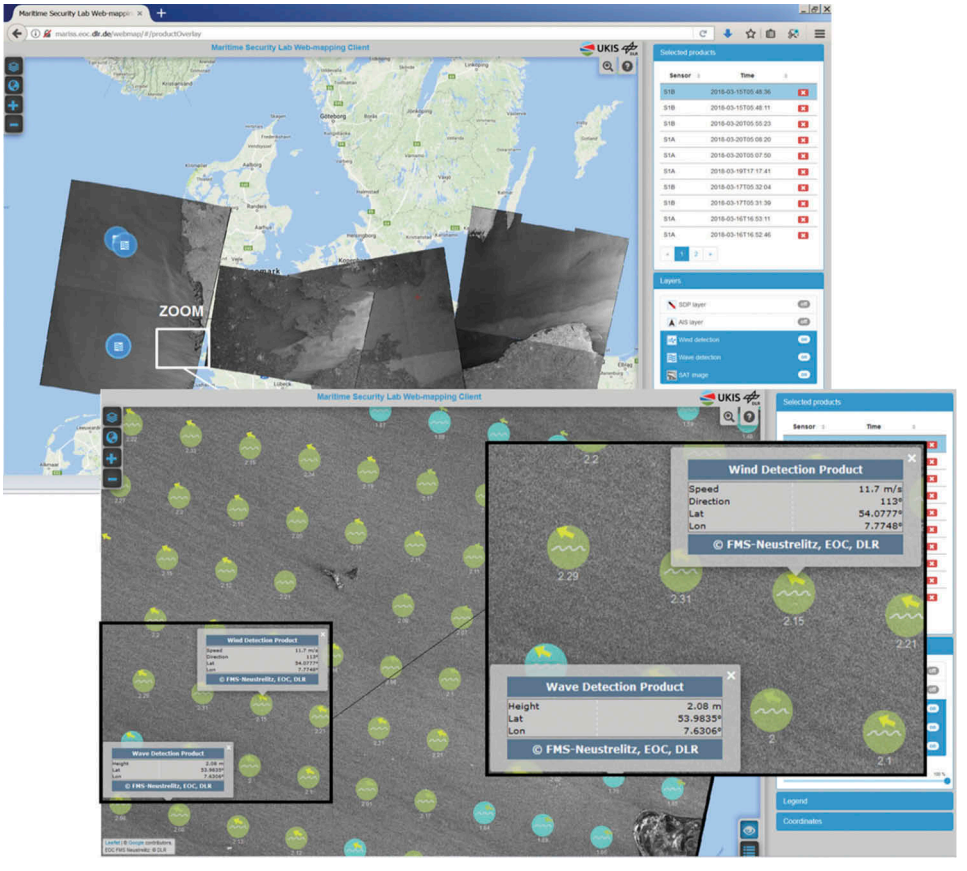

Figure 17. Screenshot of the demonstrator for NRT services at Ground Station Neustrelitz. The developed algorithm CWAVE_S1-IW is included into an integrated processor and implemented into the NRT server chain. The maritime environment: wind (arrows) and sea state (circles) and ship detection products are combined in layers. The demonstrator runs daily for Sentinel-1 IW in Southern North Sea and Western Baltic Sea.

5.3. *Copernicus local ground station Neustrelitz*

The algorithms and processors are designed for integration in NRT chain of ground station Neutsrelitz. The German Remote Sensing Data Center DFD operates the Neustrelitz Ground Station (NSG) which is used as the main ground station for reception of the high rate data stream. To support S1 reception and processing, the DFD extended the ground station to become a Local Ground Station (LGS) as part of the DLR Copernicus Collaborative Ground Segment. Located in the middle of Europe and also within the reception area of the S1 core ground stations, Neustrelitz is very suitable for receiving S1 data in a direct downlink (Pass Through) mode. The Figure 16 shows the 5° observation mask of Neustrelitz which represents the area of possible acquisitions.

The value adding Level 2 (L2) processing is performed on L1b data products. To derive S1 value added ocean products fully automated in NRT, the production is embedded in the Data Information Management System (DIMS), The PSM, developed

by DLR and Werum Software & Systems AG is used as a workflow management system to control the workflow and apply dedicated processing rules for the L1 and L2 processing. As a core processor of the framework, the SSP generates the intermediate results. Finally, multiple product formats are produced and made available in addition to the S1 L1b product. Different delivery methods are supported via e-mail (e.g. kmz, shape- and text files) or via Web Mapping Server (e.g. tiff and ESRI shape file layer) amongst others.

The DLR Ground Station Neustrelitz applies this prototype as part of an NRT demonstrator service for support of MSA. The scientific service involves the daily provision of surface wind and sea state parameters estimated full automatically from S1 IW images for the North and Baltic Seas (see Figure 17) since March 2017.

Acknowledgments

This study was supported by the German Aerospace Center (DLR) within the scope of the project 'EMSec — Real-time services for the maritime security.' Special thanks go to the German Weather Service in Hamburg for modelling data support, highly qualified advice concerning sea state and navigation and for suggestions concerning algorithm development towards practical use.

Disclosure statement

No potential conflict of interest was reported by the authors.

References

Alpers, W., and C. Brüning. 1986. "On the Relative Importance of Motion-Related Contributions to the SAR Imaging Mechanism of Ocean Surface Waves." *IEEE Transaction on Geoscience and Remote Sensing* 24: 873–885. doi:10.1109/TGRS.1986.289702.

Alpers, W., and C. Rufenach. 1979. "The Effect of Orbital Motion on Synthetic Aperture Radar Imagery of Ocean Waves." *IEEE transactions on antennas and propagation*. 27: 685–690. doi:10.1109/TAP.1979.1142163.

Ardhuin, F. , J. Stopa, B. Chapron, F. Collard, M. Smith, J. Thomson, M. Doble, et al. 2016. "Measuring Ocean Waves in Sea Ice Using SAR Imagery: A Quasi-Deterministic Approach Evaluated with Sentinel-1 and in Situ Data." *Remote sensing of environment* 189: 211–222. doi:10.1016/j.rse.2016.11.024.

Bruck, M., and S. Lehner. 2015. "TerraSAR-X/TanDEM-X Sea State Measurements Using the XWAVE Algorithm." *International journal of remote sensing* 36 (15): 3890–3912. doi:10.1080/01431161.2015.1051630.

BSH,http://www.bsh.de/de/Meeresdaten/Projekte/FINO/index.jsp

Chapron, B., H. Johnsen, and R. Garello. 2001. "Wave and Wind Retrieval from SAR Images of the Ocean." *Annales Des Telecommunications*. 56: 682–699.

CODM, COSYNA data web portal, http://kofserver2.hzg.de/codm/

Collard, F. , F. Ardhuin, and B. Chapron. 2009. "Monitoring and Analysis of Ocean Swell Fields from Space: New Methods for Routine Observations." *Journal of Geophysical Research*. 114: 15p. doi:10.1029/2008JC005215.

DataHUB, https://scihub.copernicus.eu/dhus/#/home

EMODnet, European Marine Observation and Data Network, http://www.emodnet-physics.eu/Map/#

Engen, G., and H. Johnson. 1995. "SAR-ocean Wave Inversion Using Image Cross Spectra." *IEEE Transactions on Geoscience and Remote Sensing*. 33: 1047–1056. doi:10.1109/36.406690.

ESA, 2017, ESA News: Sentinel-1 Sees through Hurricanes, http://www.esa.int/Our_Activities/Observing_the_Earth/Copernicus/Sentinel-1/Sentinel-1_sees_through_hurricanes

Etling, D., and R. Brown. 1993. "Roll Vortices in the Planetary Boundary Layer: A Review." *Boundary-Layer Meteor.* 65: 215–248. doi:10.1007/BF00705527.

Frost, A., S. Wiehle, S. Singha, and D. Krause, 2018, Sea Ice Motion Tracking from near Real Time SAR-data Acquired during Antarctic Circumnavigation Expedition. *IGARSS-2018, IEEE International Geoscience and Remote Sensing Symposium*, 23–27 July 2018, Valencia, Spain, 4p.

Hasselmann, K., and S. Hasselmann. 1991. "On the Nonlinear Mapping of an Ocean Wave Spectrum into a Synthetic Aperture Radar Image Spectrum." *Journal of Geophysical Research.* 96 (6): 10713–10729. doi:10.1029/91JC00302.

Hasselmann, K. , R. K. Raney, W. J. Plant, W. Alpers, R. A. Shuchman, D. R. Lyzenga, C. L. Rufenach, and M. J. Tucker,. 1985. "Theory of Synthetic Aperture Radar Ocean Wave Imaging: A MARSEN View." *Journal of Geophysical Research: Oceans* 90: 4659–4686. doi:10.1029/JC090iC03p04659.

Hasselmann, S. , C. Brüning, K. Hasselmann, and P. Heimbach. 1996. "An Improved Algorithm for the Retrieval of Ocean Wave Spectra from SAR Image Spectra." *Journal of geophysical research* 101–7: 16615–16629. doi:10.1029/96JC00798.

Hersbach, H. 2003, CMOD5—An Improved GMF.*ECMWF Tech. Memo. 395, Eur. Cent. for Medium-Range Weather Forecasts*, Reading, U. K

Hersbach, H., A. Stoffelen, and S. de Haan. 2007. "An Improved C-Band Scatterometer Ocean Geophysical Model Function: CMOD5." *Journal of geophysical research* 112: 16p. doi:10.1029/2006JC003743.

Holt, B. 2004. "SAR Imaging of the Ocean Surface." In *Synthetic Aperture Radar (SAR) Marine User's Manual. NOAA NESDIS Office of Research and Applications*, edited by J. Cr and A. Jr, 25–79. Washington, DC: U.S. Department of Commerce National Oceanic and Atmospheric Administration. http://www.sarusersmanual.com

Hzg. n.d. "Waves BLACKSEA." http://kofserver2.gkss.de:8080/ncWMS/godiva2.html

Karbach, M., and G. Müller. 1997. "Introduction to the Bethe Ansatz." *Computers in Physics* 11–1: 36–43. doi:10.1063/1.4822511.

Krogstad, H. 1992. "A Simple Derivation of Hasselmann's Nonlinear Ocean Synthetic Aperture Radar Transform." *Journal of geophysical research* 97: 873–885. doi:10.1029/91JC03010.

Lehner, S., A. Pleskachevsky, and M. Bruck,. 2012. "High Resolution Satellite Measurements of Coastal Wind Field and Sea State." *International journal of remote sensing* 3323: 7337–7360. doi:10.1080/01431161.2012.685975.

Lehner, S., A. Pleskachevsky, S. Brusch, M. Bruck, and M. Soccorsi,. 2014. *Remote Sensing of African Waters Using the High Resolution TerraSAR-X Satellite. Remote Sensing of the African Seas, Book, .* Heidelberg: Springer. ISBN. 978-94-017-8007-0.

Lehner, S., A. Pleskachevsky, D. Velotto, and S. Jacobsen. 2013. "Meteo-Marine Parameters and Their Variability Observed by High Resolution Satellite Radar Images." *Journal of Oceanography* 26–2: 80–91. doi:10.5670/oceanog.2013.36.

Li, X.-M., and S. Lehner,. 2014. "Algorithm for Sea Surface Wind Retrieval from TerraSAR-X and TanDEM-X Data." *IEEE Transactions on Geoscience and Remote Sensing* 52-5: 2928–2939. doi:10.1109/TGRS.2013.2267780.

Li, X.-M., S. Lehner, and T. Bruns. 2011. "Ocean Wave Integral Parameter Measurements Using Envisat ASAR Wave Mode Data." *Ieee Transactions on Geoscience and Remote Sensing* 49-1: 155–174. doi:10.1109/TGRS.2010.2052364.

Lyzenga, D. R., R. A. Shuchman, and J. D. Lyden,. 1985. "SAR Imaging of Waves in Water and Ice: Evidence for Velocity Bunching." *Journal of geophysical research* 90: 1031–1036. doi:10.1029/JC090iC01p01031.

MARNET, http://www.bsh.de/de/Meeresdaten/Beobachtungen/MARNET-Messnetz/index.jsp

Mastenbroek, C., and C. de Valk. 2000. "A Semi-Parametric Algorithm to Retrieve Ocean Wave Spectra from Synthetic Aperture Radar." *Journal of Geophysical Research* 105: 3497–3516. doi:10.1029/1999JC900282.

MSI, Marine Systems Institute, Tallinn University of Technology, METOC portal, http://on-line.msi.ttu.ee/metoc/#

NOAA, http://www.ndbc.noaa.gov/
NWSPORTAL, http://nwsportal.bsh.de/
Pleskachevsky, A., S. Lehner, and W. Rosenthal,. 2012. "Storm Observations by Remote Sensing and Influences of Gustiness on Ocean Waves and on Generation of Rogue Waves." *Ocean Dynamics* 62-9: 1335–1351. doi:10.1007/s10236-012-0567-z.
Pleskachevsky, A., W. Rosenthal, and S. Lehner. 2016. "Meteo-Marine Parameters for Highly Variable Environment in Coastal Regions from Satellite Radar Images." *Journal of Photogrammetry and Remote Sensing* 119: 464–484. doi:10.1016/j.isprsjprs.2016.02.001.
Pleskachevsky, A., S. Wiehle, S. Jacobsen, B. Tings, E. Schwarz, D. Krause, J. Kieser, and T. Bruns. 2017. "Sea State from High-Resolution Satellite-Borne SAR Imagery." *Hydrographische Nachrichten* HN 108: 34–38. 10 2017.
Ressel, R., A. Frost, and S. Lehner. 2015. "A Neural Network-Based Classification for Sea Ice Types on X-Band SAR Images." *IEEE Journal of Selected Topics in Applied Earth Observations and Remote Sensing* 8-7: 3672–3680. doi:10.1109/JSTARS.2015.2436993.
Rikka, S., A. Pleskachevsky, R. Uiboupin, and S. Jacobsen. 2018a. "Sea State in the Baltic Sea from Space-Borne High Resolution Synthetic Aperture Radar Imagery." *International journal of remote sensing* 39-4: 1256–1284.
Rikka, S., A. Pleskachevsky, S. Jacobsen, V. Alari, and R. Uiboupin. 2018b. "Meteo-Marine Parameters from Sentinel-1 SAR Imagery: Towards near Real-Time Services for the Baltic Sea." *Remote Sensing* 10-5: 757. doi:10.3390/rs10050757.
Schulz-Stellenfleth, J., T. König, and S. Lehner,. 2007. "An Empirical Approach for the Retrieval of Integral Ocean Wave Parameters from Synthetic Aperture Radar Data." *Journal of geophysical research* 112: 14p. doi:10.1029/2006JC003970.
Schulz-Stellenfleth, J., S. Lehner, and D. Hoja,. 2005. "A Parametric Scheme for the Retrieval of Two-Dimensional Ocean Wave Spectra from Synthetic Aperture Radar Look Cross Spectra." *Journal of geophysical research* 110-5: 401–417.
Schwarz, E., D. Krause, M. Berg, H. Daedelow, and H. Maas, 2015, Near Real Time Applications for Maritime Situational Awareness. *36th International Symposium on Remote Sensing of Environment, 11–15 May 2015*, Berlin, Germany Remote Sensing and Spatial Information Sciences, **vol**. **XL-7/W3**, 6p.
Shao, W., Z. Zhang, X. Li, and H. Li,. 2016. "OceanWave Parameters Retrieval from Sentinel-1 SAR Imagery." *Remote Sensing* 8, (707): 14p. doi:10.3390/rs8090707.
Singha, S., M. Vespe, and O. Trieschmann,. 2013. "Automatic Synthetic Aperture Radar Based Oil Spill Detection and Performance Estimation via a Semi-Automatic Operational Service Benchmark." *Marine pollution bulletin* 15-73 (1): 199–209. doi:10.1016/j.marpolbul.2013.05.022.
SMHI, http://www.smhi.se/en/weather/sweden-weather/sea-observations/havsvag_en.htm
Stopa, J., and A. Mouche,. 2017. "Significant Wave Heights from Sentinel-1 SAR: Validation and Applications." *JGR: Oceans* 122-3: 1827–1848.
Sun, M., Y. Yang, X. Yin, and J. Du,. 2018. "Data Assimilation of Ocean Surface Waves Using Sentinel-1 SAR during Typhoon Malakas." *International journal of applied earth observation and geoinformation* 70: 35–42. doi:10.1016/j.jag.2018.04.004.
UUS, http://on-line.msi.ttu.ee/uus_/
Wiehle, S., and S. Lehner. 2015. "Automated Waterline Detection in the German Wadden Sea Using High-Resolution TerraSAR-X Images." *Journal of Sensors* 2015: 1–6. doi:10.1155/2015/450857.

Appendix

1. Parameters for model function

For tuning and validation, a series of spectral and local parameters (Table A1) as well as GLCM-parameters (Table A2) were stored for each analysed subscene. The spectral parameters are mostly based on the integration of the image spectrum in different domains (for explanations consider the 'description' column in the tables).

GLCM is a tabulation of how often different combinations of pixel brightness values occur in an image in certain directions offset by certain distances. For the S1 IW, the NRCS were divided into 32 grey levels/numbers. Then, the combined matrix of the frequency $C(i, j)$ for different combinations of digital numbers i and j were computed and eight common GLCM features were extracted.

GLCM entropy represents spatial disorder. A completely random distribution would have very high entropy (represents chaos).

$$C_{entropy} = \sum_{i,j} C(i,j) \log(C(i,j)) \tag{A1}$$

GLCM energy is a measure of local homogeneity and is an opposite of the entropy, energy = 1 for a constant image:

$$C_{energy} = \sum_{i,j} C^2(i,j) \tag{A2}$$

GLCM contrast: A high contrast value is expected for heavy, edged textures and low for smooth, soft textures, the contrast = 0 for a constant image.

$$C_{contrast} = \sum_{i,j} i-j^2 C(i,j) \tag{A3}$$

GLCM homogeneity is a measure of the uniformity of the non-zero entries in the GLCM. If the image has little variation then homogeneity is high, homogeneity = 1 for a constant image. The range of homogeneity is [0,1].

$$C_{homogeneity} = \sum_{i,j} \frac{1}{1 + i-j^2} C(i,j) \tag{A4}$$

GLCM dissimilarity is a measure of the variation of grey level pairs in an image. It is the measure closest to contrast with a difference in the weight – contrast, unlike dissimilarity, grows quadratically. Dissimilarity range is [0,1].

$$C_{dissimilarity} = \sum_{i,j} i - j C(i,j) \tag{A5}$$

GLCM mean

$$\mu_i = \sum_{i,j=0}^{N-1} iC(i,j);\ \mu_j = \sum_{i,j=0}^{N-1} jC(i,j) \tag{A6}$$

GLCM variances

$$\sigma_i^2 = \sum_{i,j} C(i,j)(i-\eta_i)^2;\ \sigma_j^2 = \sum_{i,j} C(i,j)(j-\eta_j)^2 \tag{A7}$$

GLCM correlation:

$$C_{correlation} = \sum_{i,j} \frac{(i-_i)(j-_j)C(i,j)}{\sigma_i \sigma_j} \tag{A8}$$

Figure A1 shows an example of meteo-marine parameter estimation processed with 6 km posting using the Sea State Processor (sea state and surface wind). Figure A2 illustrates an f three basic

Table A1. Parameters extracted for each subscene based on spectral analysis together with the estimated wind speed.

Parameter	Description
M_I	Mean Intensity of subscene filtered
M_I^{dB}	Mean Intensity in Decibel, $M_I^{dB} = 10 \log M_I$
θ	Local incidence angle
E_S	Integrated Energy (k-domain 0.01 - 0.21 corresponds to wavelength 30 m - 2000 m)
E_{SF}	Integrated Energy scaled and filtered by taking into account integration angle θ_{IS}
E_{NN}	Energy integrated with noise deduction (No Noise)
E_{MAX}	Energy max in the spectrum
E_{Sk}	Energy Integrated with dividing each spectral k-bin by k^2
E_S^{100}	Integrated Energy of a spectral ring corresponding to wavelength 30 m - 100 m
E_S^{600}	Integrated Energy of a spectral ring corresponding to wavelength 100 m - 600 m
E_S^{2500}	Integrated Energy of a spectral ring corresponding to wavelength 600 m - 2500 m
N^S	Spectrum noise
N^S_{in}	Spectrum Noise inside of so-called '*cut-off*' domain of the spectrum
N^S_{out}	Spectrum Noise outside of so-called '*cut-off*' domain of the spectrum
U_{10}	Local wind speed (CMOD)

Table A2. Parameters extracted for each subscene using GLCM.

Parameter	Description
μ	GLCM mean
σ	GLCM variance
$C_{correlation}$	GLCM correlation
$C_{entropy}$	GLCM entropy
$C_{homogeneity}$	GLCM homogeneity
C_{energy}	GLCM energy
$C_{contrast}$	GLCM contrast
$C_{dissimilarity}$	GLCM dissimilarity

spectral parameters: E_S^{100}, E_S^{600}, E_S^{2500} (see Table A1) and three basic GLCM parameters: GLCM-homogeneity, GLCM-variance and GLCM-entropy (see Table A2) for an S1 IW scene presented in Figure A1.

All parameters in Tables 1A and 2A were tested for tuning; therefore both tables have a common parameter numbering. However, not all parameters were later included in the resulting model function Equation 6.

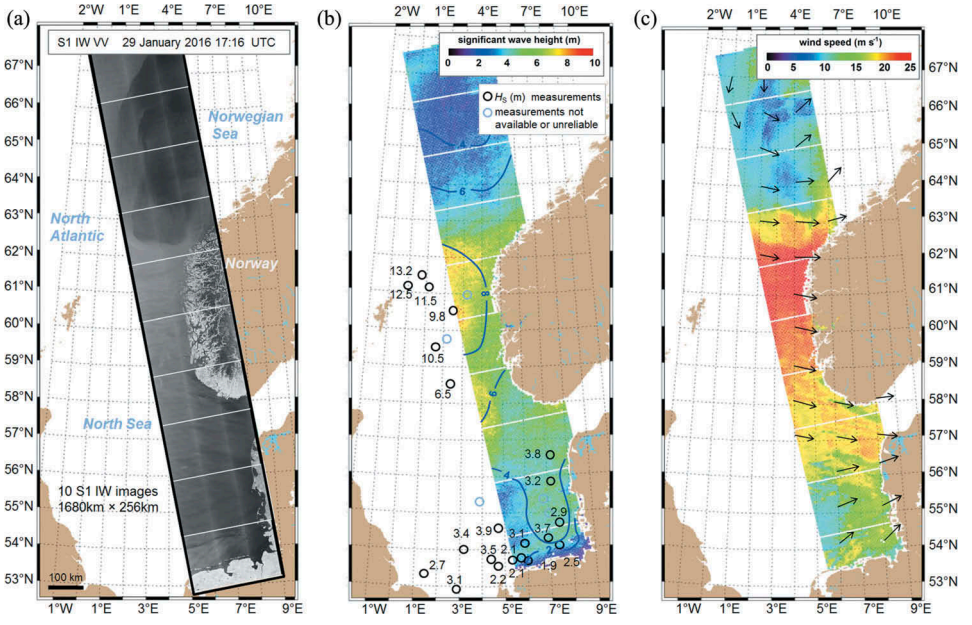

Figure A1. Example of meteo-marine parameter estimation processed with 6 km posting using the Sea State Processor with empirical CWAVE_S1-IW algorithm developed in this study. (a) S1 IW scene acquired over North Atlantic and the North Sea on 29 January 2016 under very high storm condition (WMO-8, BF-10) in the Norwegian Sea. (b) Estimated H_s. The isolines show the forecast wave model results in WWIII by NOAA. (c) Local wind speed estimated for the same subscenes using the CMOD-5 geophysical model function.

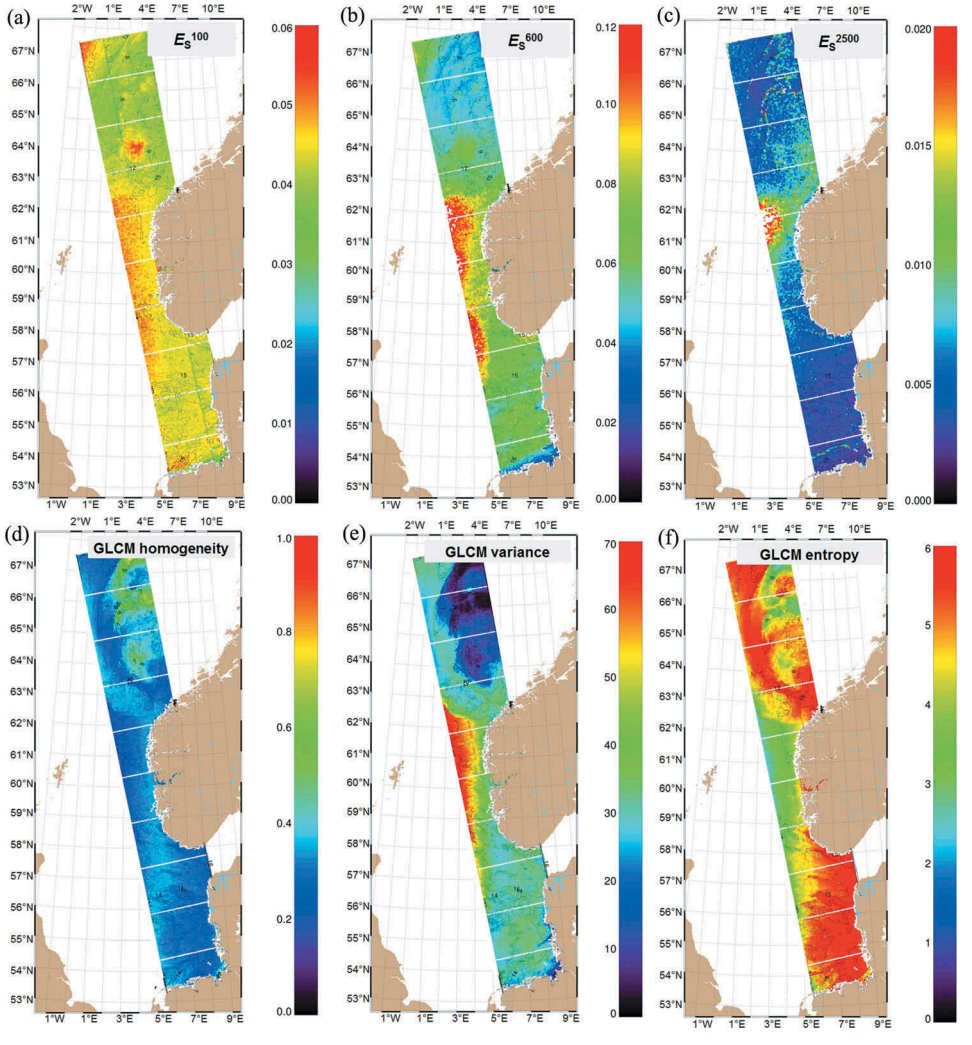

Figure A2. An example of three basic spectral parameters: (a) E_S^{100}, (b) E_S^{600}, (c) E_S^{2500} (see Table A1) and three basic GLCM parameters: (d) GLCM-homogeneity, (e) GLCM-variance and (f) GLCM-entropy (see Table A2) for a S1 IW scene.

2. Sea State Processor Details

The Sea State Processor (SSP) developed for TerraSAR-X (TS-X) SM and Sentinel-1 (S1) IW is a C++ software package integrated into the processing chain in Ground Station Neustrelitz. The current version switches the processing for TS-X and S1 images automatically. The optimal NRT workflow takes about 5-16 minutes. The information on processing timing with a pre-installed raster is shown in Table A3. In the case where a scene consists of a series of individual images, the processing runs in parallel for each image so only the acquisition time of about 2-4 minutes for S1 must be added to the total timing.

The SSP setup parameters are divided into user control parameters and model function parameters.

Model function parameters. The model function parameters are all coefficients given in this paper and parameters for the wind estimation functions XMOD-2 (for TS-X, Li, and Lehner, 2014) and CMOD-4/5 for S1 also integrated into processing chain. The wind is estimated in a separate block and requires a pre-estimated wind direction. For NRT processing, a stable input is needed working under all conditions. Since the fully automated derivation of wind direction from wind streaks on the ocean surface from the SAR images is technically not yet realized, this input is generated by the Weather Research and Forecasting (WRF) Model installed at ground station Neustrelitz. WRF reconstructs local wind fields on a grid with a resolution of 3 km using coarse data from NOAA (GFS mesh 0.5°). In case the WRF model run fails or is not available, the sea state algorithm switch automatically to a reserve wind estimation block with a *first-guess* direction of 45° that leads to an error in the wind estimation of around 1.5 m s^{-1} (order up to ca. 15%) inside SSP, but results in a smaller additional error in the wave height of about 5-20 cm.

User control. The user control parameters define the processing configuration, output setup and setup of special points (e.g. output for collocated buoys with geo-coordinates given). The most important are the following: raster step (see Tab.A3), FFT size (pre-installed 1024), the threshold for land points in an active subscene (pre-installed 5%), the threshold for the min. wind (below this value results are marked as untrustworthy, pre-installed 1.8 m s^{-1}). Less important are parameters of the outputs (e.g. output of spectra as a matrix) and plots (spectra, subscenes, etc.).

Table A3. Information on processing timing with pre-installed raster for TerraSAR-X SM and Sentinel-1 IW in ground station Neustrelitz.

Processing		TerraSAR-X SM processing time	Sentinel-1 IW processing time
acquisition and processing steps	acquisition of individual image	4 - 8 seconds	12.5 - 32 seconds
	data reception and decoding	1 – 2 minute	ca. 1 minute
	Levels L0 and L1 data processing	3 – 6 minutes	4 – 12 minutes
	Level L2 wave processing, product generation, ftp delivery	7 – 15 minutes	5 – 15 minutes
complete processing of an individual image (from the start of acquisition)		**13 – 23** minute**s**	**10 – 28** minute**s**
complete processing of scene consisting of 3 individual images (from the start of acquisition), (parallel processing)		13 – 23 minutes	10 – 28 minutes
size of pre-installed raster step for standard wave processing of subscenes 2.5 km × 2.5 km for flying direction/range direction		3 km/3 km	6 km/6 km
number of analysed subscenes for flying direction/range direction/total for an individual image for given raster step		10/15/150	40/30/1200

Results provided. The output for users can include the following files:

- all calculated parameters (Tables A1 and A2) and wave height (raster) geo-coded
- only geo-coded wave height (raster)
- geo-coded information for special points only.

On the basis of these outputs, a series of products can be processed. Currently, kmz, shape-, and text files are sent by e-mail to the users, e.g. ship cruises.